ACS APPLIED ENGINEERING MATERIALS

pubs.acs.org/acsaenm Review

Application and Progress of Graphene-Based Composite Films in Electromagnetic Interference Shielding

Daiyang Jiang, Zuhao Shi,* and Daping He*

Cite This: ACS Appl. Eng. Mater. 2025, 3, 2234−2258 Read Online

ACCESS | Metrics & More | Article Recommendations

ABSTRACT: Graphene-based composite films have emerged as promising materials for electromagnetic interference (EMI) shielding due to their excellent electrical conductivity, flexibility, and lightweight properties. As electronic devices face increasingly severe electromagnetic pollution, the development of these composite films has become particularly important. This review provides a comprehensive summary and outlook on recent developments in the field of graphene-based composite films. It systematically examines the theoretical mechanisms, fabrication methods, and various types of composite structures. Furthermore, it offers insights into the future development of graphene-based composite films. This review provides valuable insights for the specific design and performance optimization of next-generation EMI shielding solutions.

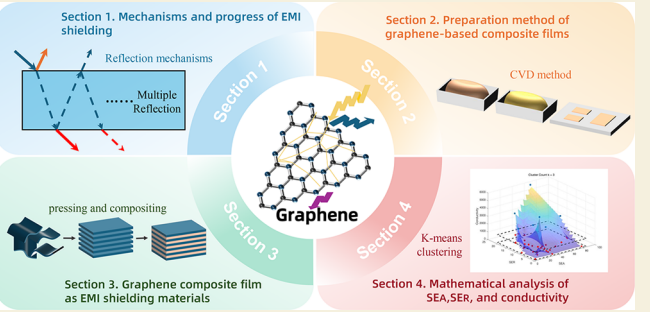

KEYWORDS: *Graphene-Based Composites, Electromagnetic Interference Shielding, Film Fabrication, Absorption Loss, Reflection Loss, Electromagnetic Wave Absorbing Materials*

1. INTRODUCTION

With the rapid development of wireless communication technology and the widespread adoption of high-frequency electronic devices across various fields, the electromagnetic environment has become increasingly complex.[1] This has intensified the issue of electromagnetic interference (EMI), as diverse electronic devices generate additional electromagnetic radiation at varying frequencies and intensities during operation. Such radiation can interfere with the normal functioning of electronic communication links and systems. Moreover, excessive electromagnetic radiation poses potential risks to human health and the environment.[2,3] Electromagnetic shielding materials, with their flexible, customizable, multifunctional, and environmentally friendly properties, have emerged as an effective solution for mitigating EMI and safeguarding the proper operation of electronic devices. Currently, various international standards and novel requirements have been established to address specific application scenarios. For instance, the MIL-STD-188-125[4] standard stipulates that materials used for nuclear electromagnetic pulse (EMP) protection must achieve a shielding effectiveness of over 80 dB and withstand extreme environments. For shielding sensitive electronic equipment, the National Security Agency (NSA) established the NSA 94−106 standard that requires shielding materials to maintain an effectiveness of at least 60−80 dB over the 1 kHz to 10 GHz frequency range. Consequently, the pursuit of high-performance electromagnetic shielding materials to meet increasingly stringent requirements has become a significant focus in materials science and electronic engineering research.

Traditional electromagnetic shielding materials primarily comprise metals such as copper, aluminum, and iron. While these materials exhibit excellent shielding effects, they also present drawbacks, including high weight, susceptibility to corrosion, challenging processing requirements, and high costs.[5] Furthermore, the high electrical conductivity of metals often leads to a shielding mechanism that predominantly relies on the reflection of electromagnetic waves.[1] This reflected radiation can easily cause secondary pollution, underscoring the need for improved solutions. A promising approach, termed the "EMI trap",[6] involves designing specialized shielding structures to reduce electromagnetic noise reflection by absorbing and dissipating electromagnetic waves, rather than relying predominantly on reflection, as with conventional materials. This approach integrates material attenuation mechanisms by combining highly conductive materials with

Received: March 17, 2025
Revised: July 17, 2025
Accepted: July 17, 2025
Published: July 26, 2025

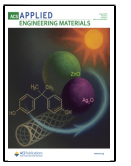

https://doi.org/10.1021/acsaenm.5c00207
ACS Appl. Eng. Mater. 2025, 3, 2234−2258

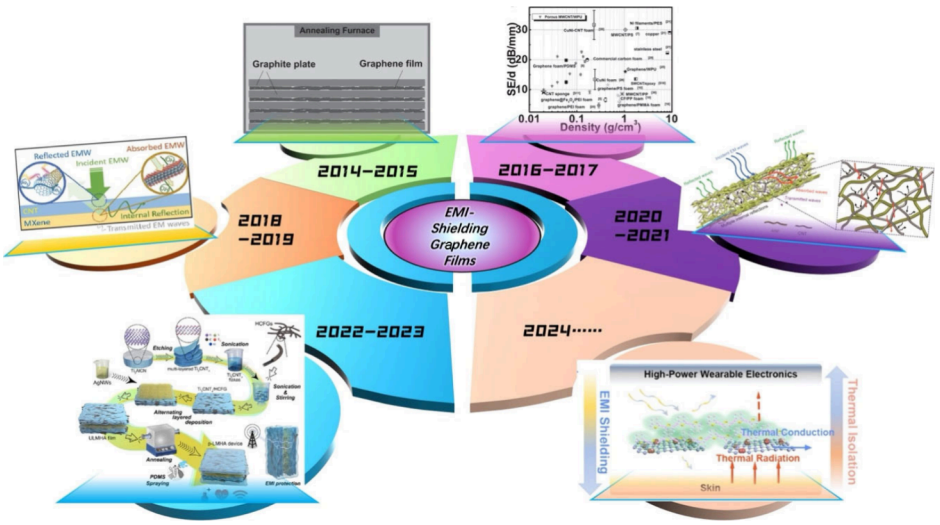

Figure 1. A review of trending articles from the past decade. [Reproduced with permission from ref 40. Copyright 2014 WILEY-VCH Verlag GmbH & Co. KGaA, Weinheim.] [Reproduced with permission from ref 173. Copyright 2015 WILEY-VCH Verlag GmbH & Co. KGaA, Weinheim.] [Reproduced with permission from ref 180. Copyright 2018 WILEY-VCH Verlag GmbH & Co. KGaA, Weinheim.] [Reproduced with permission from ref 190. Copyright 2020 America Chemistry Society.] [Reproduced with permission from ref 200. Copyright 2022 America Chemistry Society.] [Reproduced with permission from ref 203. Copyright 2024 Elsevier, Ltd.].

lossy media, such as aerogels, foams, or multilayer composite films, to achieve efficient absorption-type shielding.

Inspired by this strategy, various graphene films have gained recognition as powerful candidates for replacing traditional shielding materials due to their unique layered structure and excellent shielding efficacy. The layered structure of graphene films features abundant interfaces, which can induce multiple reflections and scattering of electromagnetic waves, thereby promoting energy absorption.[7] In 2009, a research team at Columbia University successfully synthesized high-quality graphene on copper foil via chemical vapor deposition (CVD), a method now widely employed for producing high-quality graphene films. The introduction of CVD has substantially advanced the study of graphene films.[8] Since 2010, researchers have explored the potential of combining graphene with various polymers and nanomaterials to enhance its effectiveness in electromagnetic interference shielding,[6,9,10] Additionally, with advancements in heteroatom doping technology, researchers have experimented with incorporating different heteroatoms, such as nanosilver or sulfur, into the structure of graphene or graphene oxide (GO) to develop films with high shielding performance.[11,12] Moreover, as a two-dimensional material, graphene possesses excellent loading capacity[13] and flexibility.[14] Its unique structure allows it to easily carry various substances, and its high surface area provides more binding sites (Figure 1).

As graphene-based electromagnetic shielding materials are increasingly used in high-demand fields such as wearable devices[15] and medical devices,[16] their long-term biosafety has become a key scientific challenge. The core of its safety risk lies in the fact that the graphene functional fillers may leak out of the matrix due to physical wear or aging degradation during long-term service. Existing studies have confirmed through simulation of material wear that once these leaked micro-nanoparticles enter the human body through skin contact or inhalation, they will follow the existing dose-dependent cytotoxic mechanism (such as inducing oxidative stress, damaging genetic material, etc.), posing a potential health threat.

Therefore, the biosafety of this type of composite material depends not only on the inherent toxicity of the filler but more importantly on the stability and bonding strength of the matrix coating it. Combining fillers such as graphene with natural polymer matrices such as chitosan, which have excellent biocompatibility, or firmly locking them in porous frameworks such as polyurethane, has been shown to be an effective way to ensure the safety of the overall material.[17] Currently, the cutting-edge "Safety-by-Design" concept provides a core solution for this purpose. This strategy emphasizes that by carefully modifying the surface functionalization of graphene or selecting a biocompatible matrix for compounding, its dispersibility can be improved while enhancing its shielding effectiveness and mechanical strength and significantly reducing the cytotoxicity of the material itself from the source.

This review begins with a fundamental explanation of the connection between different EMI performance metrics and test methods. Then, mainstream methods for synthesizing graphene EMI composite structures are presented. Further, the performance differences when graphene is formed into composite structures with metals or nonmetals are discussed. Finally, an analysis of key performance metrics from the high-cited papers of the past decade is given in this review. Through mathematical analysis and existing standards, the study performs regression analysis and clustering of material parameter ranges, identifying composite film categories with potential mathematical characteristics. Furthermore, the paper also offers insights into future research directions and challenges in the field of graphene-based composite films. There have been numerous excellent preliminary studies on the application of graphene in electromagnetic shielding.[18] Nevertheless, we are sure that the summarizes and outlook made in this review can give further inspiration to readers about the application of graphene-based materials in the field of EMI (Figure 2).

https://doi.org/10.1021/acsaenm.5c00207
ACS Appl. Eng. Mater. 2025, 3, 2234−2258

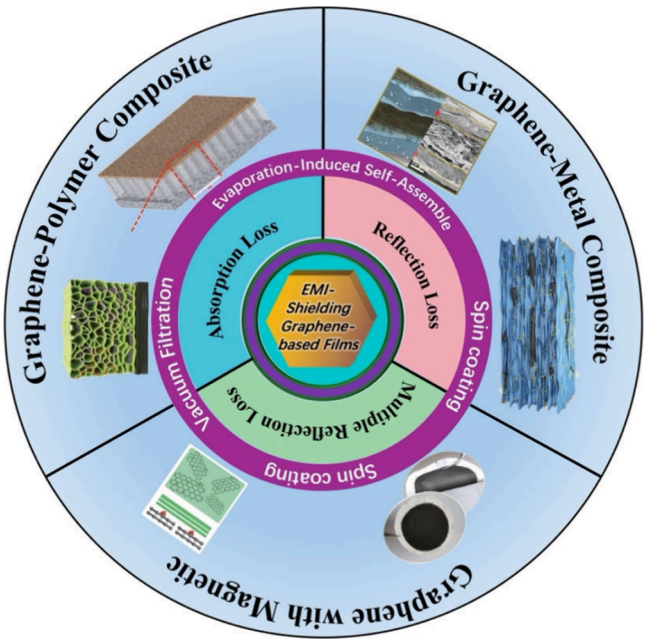

Figure 2. Overview of carbon-based composite films in EMI shielding. [Reproduced with permission from ref 193. Copyright 2020 Elsevier, Ltd.] [Reproduced with permission from ref 200. Copyright 2022 America Chemistry Society.] [Reproduced with permission from ref 203. Copyright 2024 Elsevier.] [Reproduced with permission from ref 183. Copyright 2020 The Royal Society of Chemistry.] [Modified from Ma et al.[199] under the terms of the Creative Commons Attribution International License (CC BY)].

2. MECHANISMS AND PROGRESS OF EMI SHIELDING

2.1. Main Types of EMI Shielding Mechanisms

To understand EMI shielding, we need to examine what happens when electromagnetic waves hit the shielding materials. Typically, the incident waves are first partially reflected at the surface of the material due to an impedance mismatch. The remaining parts then penetrate the material and are further attenuated by absorption and multiple internal reflections. For an effective EMI shielding material, only a very small portion of the incident wave can finally transmit through the material. To evaluate the EMI shielding capability of a material, the total shielding effectiveness (SE_T) is commonly used which is defined as the logarithmic ratios of incident power to transmitted power (eq 1):

$$SE_T = 10 \log \frac{P_T}{P_I} = 20 \log \frac{E_T}{E_I} \quad (1)$$

in which P_I, P_T, E_I and E_T represent the incident power, transmitted power, incident electric field intensity and transmitted electric field of the EM wave, respectively. According to Schelkunoff's theory, the SE_T is the sum of the reflection loss (SE_R), absorption loss (SE_A), and multiple reflection loss (SE_M). The relationship is expressed in eq 2.

$$SE_T = SE_R + SE_A + SE_M \quad (2)$$

Each type of loss can be explained and calculated by its corresponding loss mechanism; the overall mechanism is demonstrated in Figure 3a.

2.1.1. Reflection Loss. Reflection loss is a phenomenon that occurs at the surface of shielding materials when electromagnetic waves encounter the material due to an impedance mismatch. The essence of this phenomenon stems from the reflection of electromagnetic waves at the interface caused by the difference in characteristic impedance between the shielding material and the external environment. This impedance mismatch leads to energy loss when the electromagnetic waves are reflected at the surface of the shielding material. The reflection loss can be defined by the characteristic impedance of the material and the impedance of the surrounding medium (eq 3).

$$SE_R = 20 \log_{10} \left| \frac{Z_2 - Z_1}{Z_2 + Z_1} \right| \quad (3)$$

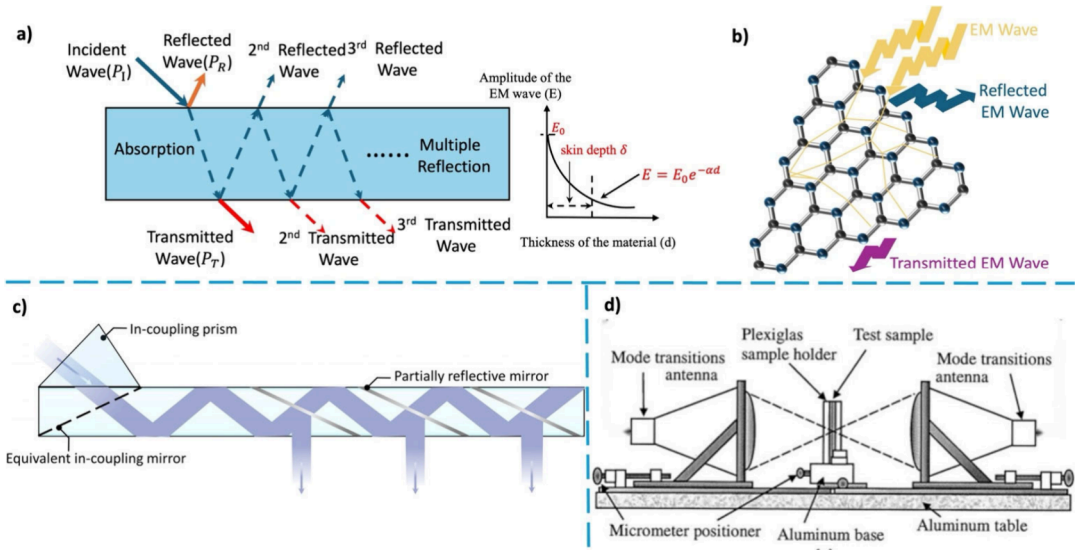

Figure 3. Mechanism of EMI shielding: (a) The interaction between incident waves and materials. (b) The microscopic mechanism of graphene in reflecting electromagnetic waves. (c) The structure of the geometric waveguide combiner. [Reproduced with permission from ref 39. Copyright 2004 Elsevier, Ltd.]. (d) Schematic configuration of the free space measurement system. [Reproduced with permission from ref 39. Copyright 2004 Elsevier, Ltd.].

https://doi.org/10.1021/acsaenm.5c00207
ACS Appl. Eng. Mater. 2025, 3, 2234−2258

Here, Z_1 represents the characteristic impedance of the surrounding medium (e.g., air), typically at approximately 377 Ω, while Z_2 is the characteristic impedance of the shielding material. The characteristic impedance Z_2 of the shielding material can be expressed in terms of the conductivity (σ), frequency (f), and permeability (μ) in eq 4:

$$Z_2 = \frac{1}{\sqrt{\sigma\mu\omega}} \quad (\omega = 2\pi f) \tag{4}$$

In the low-frequency region, since the impedance of the surrounding medium is relatively large, an approximate calculation based on low-frequency empirical formulas (eq 5) can be derived.

$$SE_R = 39.5 + 10\log_{10}\left(\frac{\sigma}{2\pi f\mu}\right) \tag{5}$$

In practical applications, reflection loss is one of the key parameters for evaluating the effectiveness of electromagnetic shielding. For highly efficient electromagnetic shielding materials, it is essential to create a significant impedance mismatch at the interface between the shielding material and the surrounding medium, thereby achieving high reflection loss and reducing the conduction of electromagnetic waves within the material. Researchers have found that pyrolyzing polyacrylonitrile/SiCN fibers at 800 °C can result in good impedance matching, with the material's reflection loss reaching 10 dB (indicating that 90% of the electromagnetic waves are reflected).[19]

2.1.2. Absorption Loss. The phenomenon of absorption loss occurs when electromagnetic waves penetrate shielding materials, where interactions with the material's molecules, atoms, and free electrons cause the intensity of the electromagnetic wave, E, to decay exponentially (i.e., $E = E_0\, e^{-\alpha d}$ in a shielding material with thickness d). This attenuation can be quantified by the material's attenuation constant (α), which can be expressed as a function of the shielding material's angular frequency (ω), magnetic permeability (μ), electrical conductivity (σ), and dielectric constant (ε) in eq 6.

$$\alpha = \omega\sqrt{\frac{\mu\varepsilon}{2}\left[\sqrt{1+\left(\frac{\sigma}{\omega\varepsilon}\right)^2} - 1\right]} \tag{6}$$

To achieve higher absorption loss, it can be seen from the equation that enhancing the material's electrical conductivity, dielectric constant, and magnetic permeability is effective. Materials with high electrical conductivity produce stronger ohmic losses, allowing electromagnetic wave energy to be converted into heat more rapidly.[20] By enhancing effects such as electric dipole polarization and interfacial polarization,[21] the polarization of electromagnetic waves within the material can be increased, thereby improving absorption loss. Hysteresis and eddy current losses accelerate the dissipation of electromagnetic wave energy,[22] similarly leading to a faster conversion into heat. Also, the thicker the material, the longer the propagation path of the electromagnetic waves within the material, and the more energy is lost.[23] The SE_A can be expressed in eq 7 for conducting shielding materials.

$$SE_A = 20\log_{10} e^{\alpha d} = 8.686\left(\frac{d}{\delta}\right) = 8.686d\sqrt{\pi f\mu\sigma} \tag{7}$$

δ is the skin depth. It is defined as the depth at which the electric field strength decays to e^{-1} of its original value. Toward a conduct shield, skin depth can be expressed as $\delta = \frac{1}{\alpha} = \frac{1}{\sqrt{\pi f\mu\sigma}}$. And d is the thickness of the material. The thickness and electrical conductivity contribute majorly toward absorption while permeability and dielectric constant determines absorption loss.[24] Studies have found that a nickel/carbon foam material synthesized via a green and simple one-pot method, possessing high electrical conductivity and magnetism, achieved a reflection loss of 45 dB at a frequency of 13.3 GHz with a thickness of 2 mm, demonstrating excellent microwave absorption capabilities.[25]

2.1.3. Multiple Reflection Loss. Multiple reflection loss is similar to reflection loss. When electromagnetic waves pass through shielding materials with multilayered or porous structures, each reflection causes a portion of the energy to be dissipated or absorbed, resulting in a gradual attenuation of the transmitted electromagnetic wave energy. In thin shielding materials, back reflection affects the final transmission, as the reflected wave is re-reflected at the front surface and contributes to a second transmission, until the energy is completely dissipated. SE_M is calculated by eq 8.

$$SE_M = 20\log_{10}(1 - e^{-2\alpha d}) \tag{8}$$

SE_M is closely related to the material thickness. When the thickness of the shielding material approaches δ, the impact of SE_M becomes negligible ($\alpha d \ll 1$). At this point, $1 - e^{-2\alpha d}$ can be approximated as $2\alpha d$. Therefore, SE_M can be expressed in eq 9.

$$SE_M \approx 20\log_{10}(2\alpha d) = 20\log_{10}(2d\sqrt{\pi f\mu\sigma}) \tag{9}$$

2.1.4. Internal Scattering. Internal scattering occurs at interfaces with an impedance mismatch. These interfaces lead to additional scattering within the material, often referred to as internal multiple reflections.[26] Internal scattering increases the interaction between the electromagnetic waves and the material, extending the propagation path of the waves within the material and further promoting energy dissipation.[27] Unlike reflection loss, internal scattering primarily depends on the material's microstructure and internal characteristics, rather than being caused by interface reflections. Therefore, internal scattering contributes to enhanced absorption loss, particularly in porous or heterogeneous materials, significantly improving the shielding effectiveness. The overall internal scattering can be described as $\sigma_s \times d$ (σ_s is the scattering cross-section, which describes the scattering loss per unit volume).

The impedance matching of interfaces and the ability to dissipate electromagnetic waves determine the wave absorption performance of the absorbing materials. Although doping graphene with heteroatoms,[28−31] adjusting its structure, and optimizing its morphology can improve the impedance matching of graphene materials, challenges such as low magnetic permeability, impedance mismatch, and limited loss mechanisms remain significant hurdles in the development of graphene-based materials. An ideal wave-absorbing material should incorporate multiple electromagnetic loss mechanisms.[32] The microscopic mechanism of graphene in reflecting electromagnetic waves is shown in Figure 3b. To enhance the wave absorption performance of graphene, extensive research has been conducted, focusing on various loss mechanisms. By strategically introducing additional components (e.g., carbon

https://doi.org/10.1021/acsaenm.5c00207
ACS Appl. Eng. Mater. 2025, 3, 2234−2258

nanotubes, magnetic metals, ferrites, polymers), the wave-absorbing capacity of graphene-based composites can be significantly improved.

2.2. Three Main Experimental Measurement Techniques of EMI SE

The measurement of EMI SE primarily focuses on the reflection, transmission, and attenuation of electromagnetic waves to assess the material or device's ability to suppress electromagnetic interference. We need to analyze the reflection and transmission characteristics of the material under test (MUT) across different frequency bands, which can be represented by parameters such as the reflection coefficient, transmission coefficient, and others. In the laboratory, a Network Analyzer (NA) is typically used for measurement. NA can be divided into two types: Scalar Network Analyzer (SNA) and Vector Network Analyzer (VNA).[33] An SNA generally measures only the amplitude of the signal, while a VNA can also measure the phase of the signal, as well as the complex permittivity (ε^*)[34] and complex permeability (μ^*).[35]

In a two-port VNA, the incident and transmitted signals can be represented by *S*-parameters (scattering parameters). The *S*-parameters include the reflection coefficient (S_{11} or S_{22}) and the transmission coefficient (S_{12} or S_{21}), while the shielding effectiveness is calculated based on these reflection and transmission coefficients. The reflection (R) and transmission (T) are given by $R = |S_{11}|^2 = |S_{22}|^2$ and $T = |S_{12}|^2 = |S_{21}|^2$.[36] In addition to the basic shielding effectiveness, the VNA can also help estimate the SE_R and SE_A, which are then used to further calculate the overall EMI SE of the material. Using the *S*-parameters, the EMI SE can be expressed in eqs 10−12:

$$SE_T = 10 \lg\left(\frac{1}{T}\right) \tag{10}$$

$$SE_R = 10 \lg\left(\frac{1}{1-R}\right) = 10 \lg\left(\frac{1}{1-|S_{11}|^2}\right) \tag{11}$$

$$SE_A = 10 \lg\left(\frac{1-R}{T}\right) = 10 \lg\left(\frac{1-|S_{11}|^2}{|S_{21}|^2}\right) \tag{12}$$

There are three main experimental measurement methods for the EMI SE.

2.2.1. Waveguide Method. The waveguide method is a technique used to assess the SE of materials against electromagnetic waves through a waveguide structure. The material under test is placed within a waveguide device, allowing electromagnetic waves to propagate through the waveguide.[37] The shielding effectiveness is then calculated by measuring the difference in signal strength between the waveguide's input and output. The waveguide method can accurately evaluate the material's shielding performance across different frequency ranges and wavelengths, offering high precision and broad applicability (Figure 3c).

2.2.2. Coaxial Airline Method. The SE is evaluated by making the MUT into a rectangular toroidal shape and inserting it between the inner and outer conductors of a coaxial cable structure, then measuring the attenuation of the signal after it passes through the material.[38] This method is applicable to almost all frequency ranges; however, due to the requirement that the toroidal sample be very thin, careful preparation by the experimenters is necessary.

2.2.3. Free Space Method. The free space method is particularly suitable for inhomogeneous or anisotropic materials. In this method, the MUT is placed in free space, and precise focusing horn antennas are used for signal transmission and reception[39] (Figure 3d). The S_{11} and S_{21} are measured to determine the complex permittivity and loss tangent of the composite material. This method eliminates the need for precise sample machining, is applicable for measurements under extreme temperature conditions, and avoids the excitation of higher-order modes.

2.3. The Key Role and Implementation of Graphene Orientation in Electromagnetic Shielding

In fact, the orientation of graphene sheets within the composite film is a key parameter for optimizing the EMI SE. In comparison to randomly oriented structures, highly ordered and oriented structures are conducive to the formation of continuous and efficient conductive networks. This anisotropic alignment significantly reduces the junction resistance between adjacent graphene sheets, thereby providing an uninterrupted path for electron transport.[40] Therefore, the mobility of the carriers is enhanced, thereby enhancing the interaction with the incident electromagnetic waves. This manifests itself as an increase in reflection losses (due to efficient carrier response) and absorption losses (due to enhanced ohmic losses as the current propagates in the conductive network). Therefore, precise control of graphene orientation is a key strategy to maximize its inherent high conductivity to achieve excellent EMI shielding performance.[41]

Several key methods have been developed to achieve a high orientation of graphene. Mechanical force-induced orientation is one of the most general and scalable methods. Techniques such as doctor blade, spin coating, and flow-assisted assembly (FAA) use shear forces to force graphene or GO flakes to align in a planar co-oriented manner, parallel to the substrate or flow direction.[42] Similarly, mechanical stretching of graphene−polymer composite films can effectively orient the embedded flakes along the stretching direction.[43] Field-induced orientation provides another effective approach, where an external magnetic or electric field is applied to the graphene dispersion. This method uses the diamagnetic anisotropy of GO or the surface charge on the flakes to guide their orientation before the matrix solidifies.[44] In addition, some advanced self-assembly strategies, such as the formation of liquid crystal (LC) phases at high GO concentrations or the Langmuir−Blodgett (LB) technique, can produce very well-ordered monolayer or multilayer films, although they are usually limited in scalability.[45] Therefore, the selection of an appropriate orientation method is a critical consideration, which needs to balance the desired degree of order with the practical requirements of the application and manufacturing process.

3. PREPARATION METHOD OF GRAPHENE-BASED COMPOSITE FILM

Although graphene films possess excellent electrical conductivity and mechanical strength, they are difficult to directly use as electromagnetic shielding materials due to insufficient film thickness, uneven shielding efficiency, and limited tunability. To address this issue, researchers typically combine graphene with other materials, such as metals, conductive polymers, and carbon nanotubes, to form graphene-based composite films. These composite films are thin films

https://doi.org/10.1021/acsaenm.5c00207
ACS Appl. Eng. Mater. 2025, 3, 2234−2258

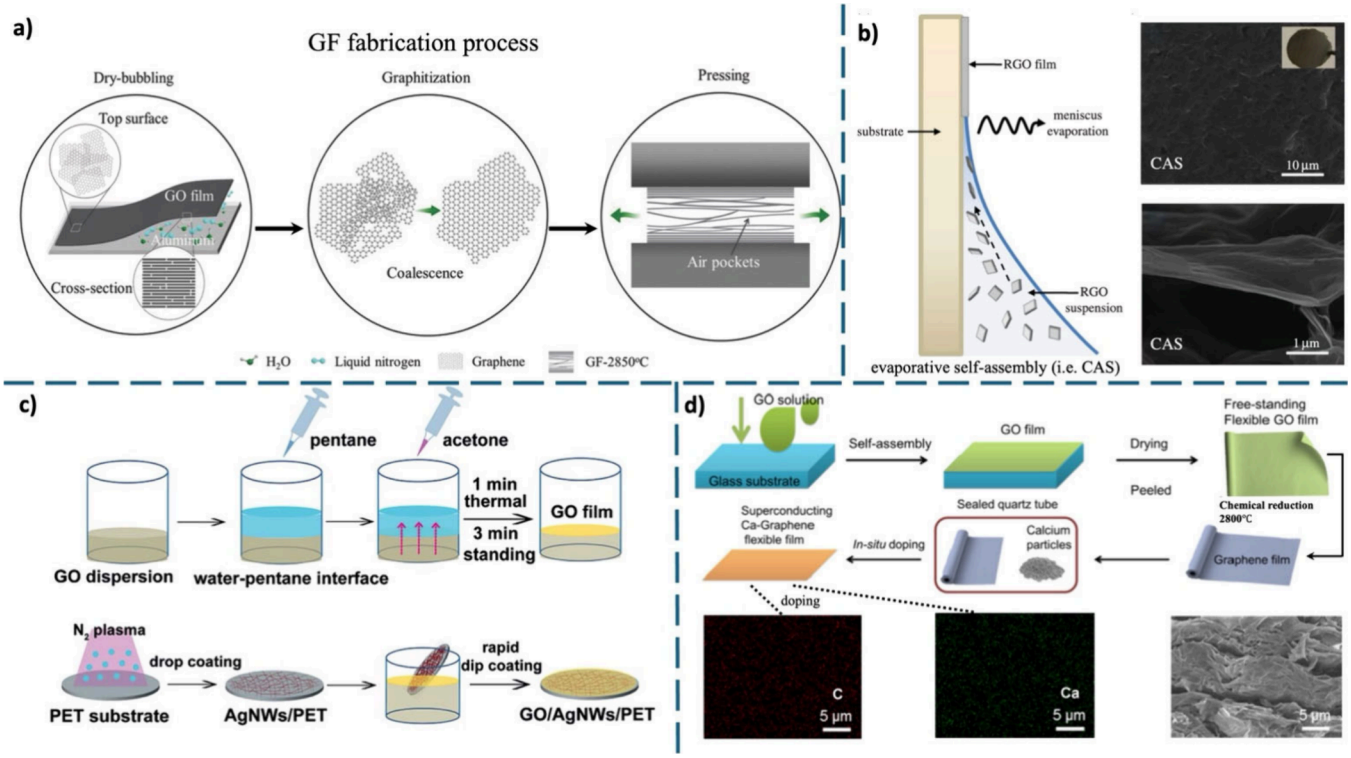

Figure 4. (a) Fabrication of the GO films via evaporation-induced self-assembly [Reproduced with permission from ref 48. Copyright 2018 WILEY-VCH Verlag GmbH & Co. KGaA, Weinheim]. (b) The schematic of techniques for preparing graphene membranes on nylon supports via evaporative self-assembly [Reproduced with permission from ref 49. Copyright 2015 the Royal Society]. (c) Preparation of the GO film and the GO/AgNW/polyethylene terephthalate (PET) electrode. [Modified from Wu et al.[51] under the terms of the Creative Commons Attribution International License (CC BY)]. (d) Schematic illustration of the fabrication process of Ca-GSF [Reproduced with permission from ref 52. Copyright 2019 Elsevier, Ltd.].

composed of graphene or graphene derivatives combined with other materials that incorporate the superior properties of graphene and exhibit enhanced electromagnetic wave absorption and reflection capabilities. Additionally, graphene-based composite films show great potential for widespread applications in various fields, such as gas and liquid separation, desalination, sensors, electronic devices, and biomedicine,[46] Here we introduce four main preparation methods for graphene-based films, including evaporation-induced self-assembly, vacuum filtration, blade coating, and spin coating.[47]

3.1. Evaporation-Induced Self-Assembly

The evaporation-induced self-assembly (EISA) technique primarily leverages solvent evaporation to drive the alignment of graphene sheets, thereby forming uniform and dense films on substrates. Wang et al.[48] employed the traditional evaporation-induced self-assembly technique to fabricate graphene films. They initially expanded and aligned the GO films through dry-bubbling treatment, followed by high-temperature graphitization to improve the quality and alignment (Figure 4a). Finally, mechanical pressing was applied to remove air pockets and enhance the film's strength. The resulting graphene films exhibited excellent thermal conductivity (approximately 3200 W/m·K) and mechanical properties. This method is also extensively employed for the large-scale fabrication of uniform and ordered films.[49,50] Similarly inspired by this method, Sheath and Majumder[49] fabricated RGO membranes using capillary-force-assisted self-assembly (CAS) combined with vacuum filtration (Figure 4b). The membranes produced by the CAS technique exhibited higher molecular order, demonstrating better filtration performance and higher water flux. In addition, Wu et al.[51] utilized a rapid self-assembly process at the pentane-water interface to produce ultrathin and uniform GO films, as depicted in Figure 4c. These films were successfully applied as protective layers for silver nanowire (AgNW) transparent electrodes. By adjusting the amount of acetone injected and the self-assembly duration, large area GO films were formed within 3 min. Upon coverage of the AgNW, the sheet resistance was reduced by approximately three-four times, while the transmittance decreased by only 2%. This GO/AgNW composite film exhibits high electrical conductivity and stability, making it suitable for use in flexible electronic devices.

In addition to evaporation-induced self-assembly, studies have also prepared large-area graphene-based superconducting films (GSF) that can be cut into any desired shape by combining self-assembly with in situ calcium intercalation technology.[52] (Figure 4d) Other studies have combined self-assembly techniques with high-temperature graphitization to produce copper/graphene films with high tensile strength (over three times that of commercial polymer gel sheets).[53]

3.2. Vacuum Filtration

The vacuum filtration method typically begins by dispersing and mixing graphene or GO nanosheets to achieve a uniform dispersion. This dispersion is then subjected to vacuum filtration, causing the nanosheets to deposit onto the filter membrane and form a dense film. Finally, the film is dried and peeled off to obtain free-standing film.[54]

https://doi.org/10.1021/acsaenm.5c00207
ACS Appl. Eng. Mater. 2025, 3, 2234−2258

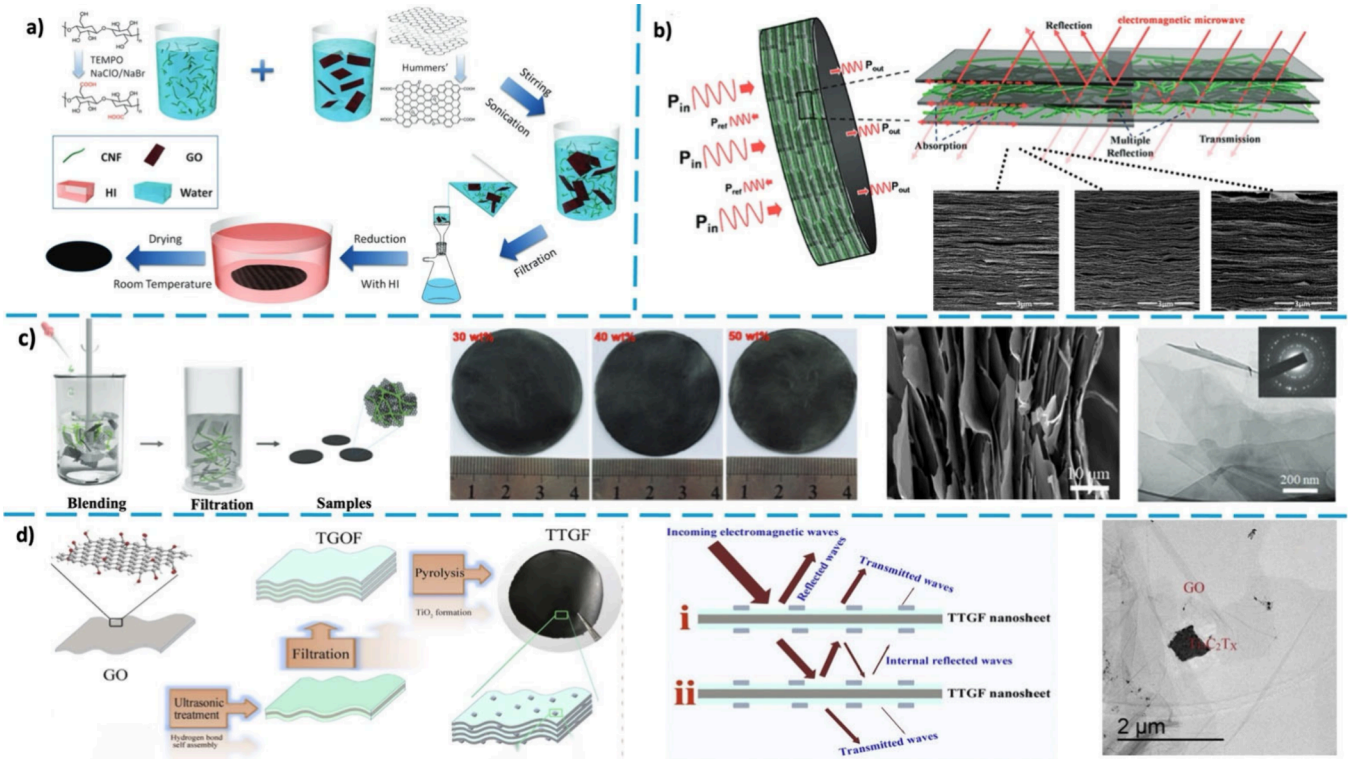

Figure 5. Schematic illustration of the (a) fabrication of RGO/CNF composite films and the (b) microwave transfer across the composite films. [Reproduced with permission from ref 56. Copyright 2017, The Royal Society of Chemistry.]. (c) Highly flexible biodegradable cellulose nanofiber/graphene heat-spreader films via simple vacuum-assisted filtration. [Reproduced with permission from ref 57. Copyright 2018, The Royal Society of Chemistry.]. (d) Lightweight and ultrathin TiO_2−$Ti_3C_2T_X$/graphene film by a vacuum filtration and pyrolysis method. [Reproduced with permission from ref 58. Copyright 2018, Elsevier, Ltd.].

Since Dikin et al.[55] first prepared standalone GO paper via vacuum filtration in 2007, this method has been widely employed in numerous academic studies. Yang et al.[56] utilized a vacuum-assisted filtration method combined with hydrogen iodide (HI) reduction treatment to fabricate reduced graphene oxide/cellulose nanofiber (RGO/CNF) composite films (Figure 5a). The structure and microwave transfer progress are shown in Figure 5b. Similarly, Chen et al.[57] fabricated highly thermally conductive flexible cellulose nanofiber/graphene composite films using a vacuum-assisted filtration method. This technique utilizes the highly ordered hierarchical structure of graphene nanosheets, imparting excellent heat-spreading performance and good flexibility to the composite films. The composite film containing 50 wt % graphene achieved an in-plane thermal conductivity of 164.7 W/m·K, with a through-plane thermal conductivity of 5.0 W/m·K. Moreover, the thermal conductivity of the film remained almost unchanged after 1000 bending cycles. This method not only significantly enhances the thermal conductivity of cellulose-based composite films but also provides superior mechanical properties and flexibility, making them suitable as heat-spreader materials for flexible electronic devices. Their findings are illustrated in Figure 5c. Xiang et al.[58] also developed a lightweight and ultrathin TiO_2−$Ti_3C_2T_X$/graphene film for EMI shielding. The film was fabricated using vacuum-assisted filtration and pyrolysis, with a thickness ranging from 5.25 to 9.17 μm. The TiO_2−$Ti_3C_2T_X$/graphene film exhibited excellent electrical conductivity and EMI SE, with the EMI SE of the TiO_2−$Ti_3C_2T_X$ /graphene composite reaching 27 dB. Considering the material's density and thickness, the specific shielding effectiveness per thickness (SSE/t) was 30291.43 dB cm^2 g^{-1}, demonstrating the film's high efficiency in absorbing electromagnetic radiation (Figure 5d), while maintaining its low weight and ultrathin structure.

3.3. Blade Coating and Roll to Roll Progress

The blade coating method starts with preparation of GO dispersion, which is similar to the vacuum filtration method. This dispersion is then poured onto a flat substrate and spread evenly by using a blade, during which the thickness of the resulting film can be controlled by the height of the blade. The obtained GO films then undergo reduction processes for improved conductivity and sometimes compression treatment for better structural stability.[59−62] The fabrication, mechanical pressing process, and image of the GFs via blade coating and relevant technologies are illustrated in Figure 6a.

Liu et al.[63] developed a method for rapidly producing graphene films using intensive Joule heating combined with a roll-to-roll and blade coating process (Figure 6b). The process involves passing chemically rGO films through rotating graphite rollers while applying current to heat the films to high temperatures. This method significantly reduces the energy consumption and processing time. The resulting graphene films exhibit excellent thermal conductivity (1285 ± 20 W/m·K) and electrical conductivity (4.2×10^5 S/m), making them promise for thermal management applications. This approach provides a promising solution for the large-scale production of high-performance graphene films. In addition, Si et al.[64] developed a roll-to-roll processable MXene-rGO-poly(vinyl alcohol) (PVA) composite film with enhanced mechanical properties and environmental stability, suitable for EMI shielding. The composite film was fabricated by using a

https://doi.org/10.1021/acsaenm.5c00207
ACS Appl. Eng. Mater. 2025, 3, 2234−2258

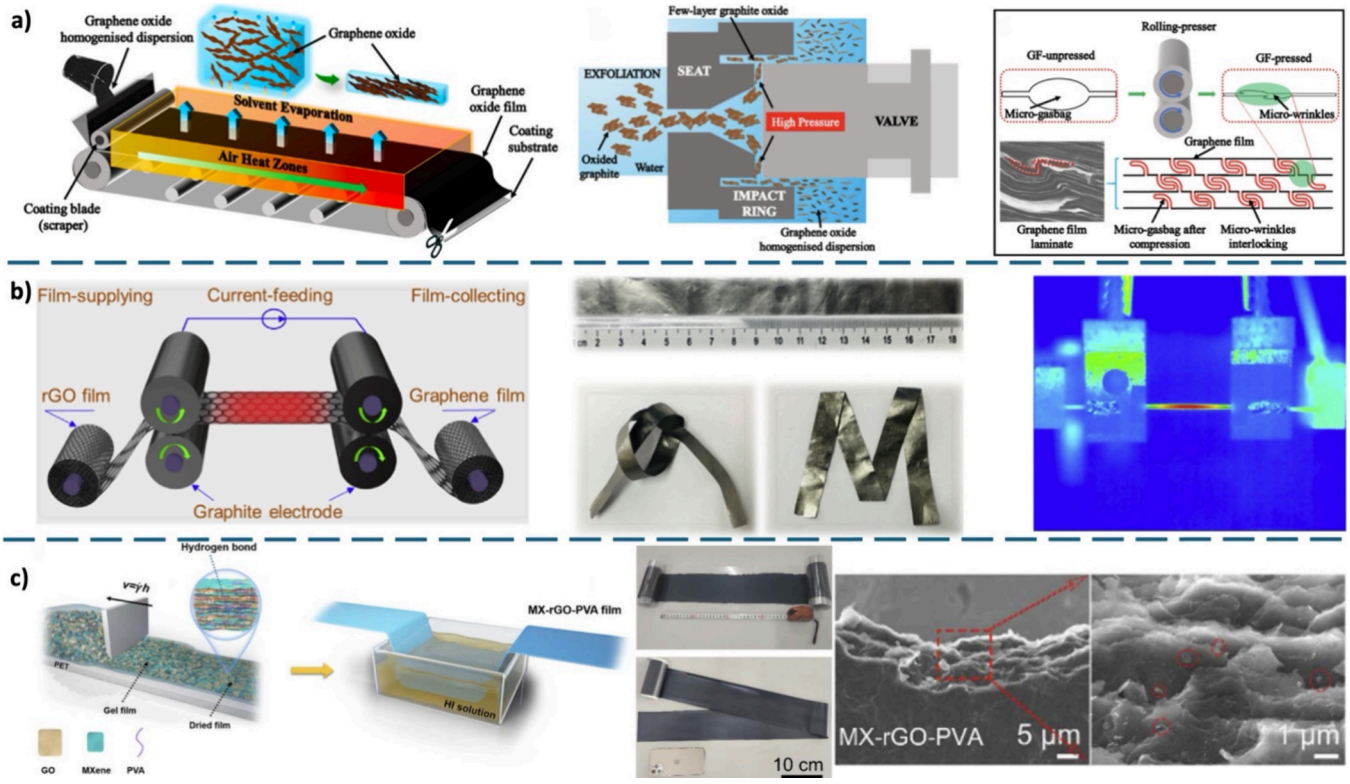

Figure 6. (a) Ultrathick graphene film for pyrolytic graphite film via blade coating method. [Reproduced with permission from ref 62. Copyright 2020 Elsevier, Ltd.]. (b) Rapid roll to roll production and blade coating of graphene film with intensive Joule heating. [Reproduced with permission from ref 63. Copyright 2019 Elsevier, Ltd.]. (c) Roll-to-roll processable MXene-rGO-PVA composite films by a simple blade casting method. [Reproduced with permission from ref 64. Copyright 2022 Elsevier, Ltd.].

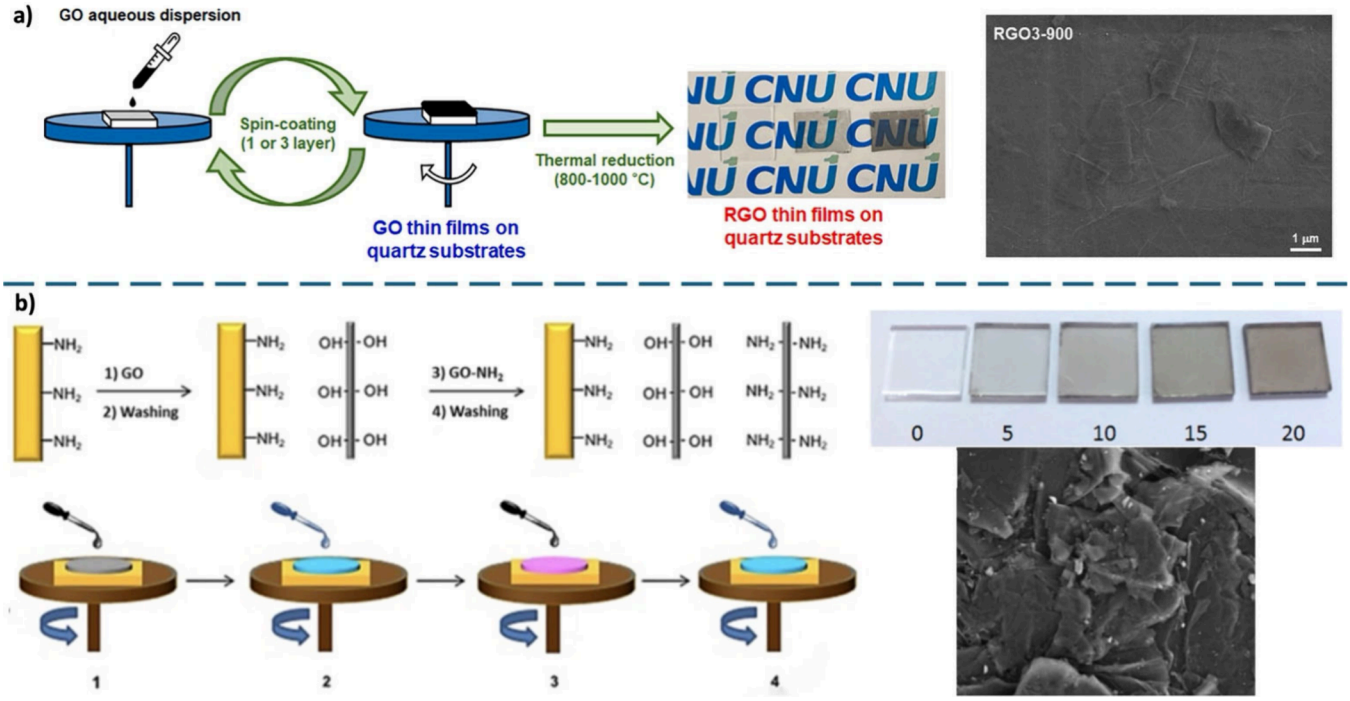

Figure 7. (a) Fabrication of the RGO thin films on quartz substrates via spin-coating and thermal reduction. [Modified from Kim et al.[66] under the terms of the Creative Commons Attribution International License (CC BY)]. (b) Spin-assisted LBL process to prepare transparent conductive rGO films. [Reproduced with permission from ref 68. Copyright 2019 Elsevier, Ltd.].

blade-coating technique through the cooperative assembly of $Ti_3C_2T_X$, MXene, rGO, and PVA. This structure provides the composite film with high tensile strength (approximately 238 MPa) and toughness (approximately 1.72 MJ/m^3), along with excellent electrical conductivity (approximately 32 S/cm). With a thickness of 12 μm, the film demonstrates an EMI SE of

https://doi.org/10.1021/acsaenm.5c00207
ACS Appl. Eng. Mater. 2025, 3, 2234−2258

41.35 dB, with an absolute shielding effectiveness of approximately 20,200 dB cm^2/g (Figure 6c). Moreover, the composite film maintains stable EMI shielding performance and mechanical strength under extreme conditions, such as sonication, hot/cold annealing, and acidic solutions. The excellent performance of this composite film provides strong support for its large-scale production and practical applications.

3.4. Spin Coating

Spin coating is a widely utilized and efficient technique for the fabrication of graphene membranes, capable of uniformly depositing graphene dispersions onto substrates within a short time frame through centrifugal force, thereby forming continuous thin films. The preparation process typically involves dispersing GO or its functionalized derivatives in a solvent and adjusting the viscosity by controlling the concentration. Subsequently, the solution is deposited onto a substrate (e.g., glass, PET, or quartz) and uniformly spread via spin coating to produce a consistent GO film.[65−67]

The fabrication process of the spin coating method to prepare thin RGO films is illustrated in Figure 7a. Moreover, the layer-by-layer (LBL) assembly technique is frequently combined with a spin coating. Through electrostatic or hydrogen bonding interactions, materials with opposite charges (e.g., cellulose nanocrystals and GO) are alternately deposited to construct multilayer structures, thereby enhancing the mechanical strength and electrical conductivity of the films.[68−70] Oytun et al.[68] prepared transparent conductive rGO films with an optical transmittance of 75% on glass substrates using a spin-assisted deposition method (Figure 7b). This method involved the alternate deposition of oppositely charged GO and amine-functionalized graphene oxide (GO-NH_2).

3.5. Summary of the Preparation Methods

In the fabrication of graphene-based composite films, several methods have been developed, each offering unique advantages and limitations. Traditional techniques mentioned above are widely used for producing uniform and high-performance films. EISA allows for precise control over film formation, resulting in uniform and ordered films ideal for applications requiring high electrical conductivity and mechanical strength; however, it requires meticulous control over solvent evaporation and can be time-consuming. Vacuum filtration is a straightforward process suitable for uniform film production but faces challenges in controlling film thickness and uniformity, especially in large-scale production. Blade coating is scalable for mass production but struggles with precise thickness control and film uniformity, while spin coating, commonly used for small-area, high-precision applications, faces limitations in large-area fabrication due to uniformity issues. All the information about these four methods is illustrated in Table 1.

In addition to these traditional methods, emerging techniques, such as the sol−gel method, spray coating, laser-induced graphitization, and electrospinning, have shown significant promise. The sol−gel method[71−73] offers excellent control over film porosity and thickness, though it is sensitive to precursor selection and may lead to surface nonuniformity during heat treatment. Spray coating[74−76] is a simple and scalable technique, ideal for large-area production, but it requires careful control over solution concentration and equipment to ensure uniformity. Laser-induced graphitization[77−79] provides high precision and the ability to create high-

Table 1. Summary of the Four Main Fabrication Methods

Preparation method	Key Principle Description	Key Benefits	Main limitations	Typical Applications/ Advantages	refs
Evaporation-induced self-assembly	Solvent evaporation drives the alignment of graphene sheets to form a uniform and dense film.	Precisely control film formation, highly uniform and orderly films; High thermal conductivity (~3200 W/m·K) and mechanical properties; Suitable for large-scale preparation of ordered thin films; CAS and vacuum filtration can be combined to improve filtration performance; Rapid preparation of ultrathin uniform GO films for transparent electrodes; Can be combined with in situ doping to prepare superconducting thin films.	Solvent evaporation parameters need to be carefully controlled; The process may be time-consuming.	High-order thin films, thermal management, filtration, transparent electrodes, superconductors	48−53
Vacuum filtration	The graphene/GO nanosheet dispersion is deposited on the filter membrane by vacuum adsorption to form a dense film.	Simple process, suitable for uniform film production; Widely used in academic research; Can be combined with reduction treatment to enhance performance; Preparation of highly thermally conductive flexible composite films suitable for heat dissipation materials; Prepare lightweight ultrathin EMI shielding film, high EMI SE (27 dB), high SSE/t (30291.43 dB cm^2 g).	Difficult to precisely control film thickness and uniformity, especially in large-scale production.	Self-supporting films, thermal management, lightweight EMI shielding	54−58
Doctor coating and roll-to-roll processes	GO dispersion is poured onto the substrate and spread evenly with a scraper. The thickness is controlled by the scraper height..	Highly scalable and suitable for large-scale production; Combined with Joule heating to achieve fast and energy-saving production; High thermal conductivity (1285 ± 20 W/m·K) and electrical conductivity (4.2×10^5 S/m); Enhanced mechanical properties and environmental stability (tensile strength ~238 MPa); High EMI SE (41.35 dB), stable performance under extreme conditions.	Difficult to precisely control film thickness and uniformity over large areas.	Industrial scale production, thermal management, robust EMI shielding	59−64
Spin coating	graphene dispersion is uniformly deposited onto the substrate by centrifugal force to form a continuous film.	High efficiency, small area uniform deposition in a short time; Can be combined with layer-by-layer (LBL) assembly to enhance mechanical strength and conductivity; Transparent conductive rGO film can be prepared (75% transmittance).	There are uniformity issues in large-area preparation; Mainly used for small area, high precision applications.	Thin film devices, transparent electronic products, sensors, interface engineering	65−70

https://doi.org/10.1021/acsaenm.5c00207
ACS Appl. Eng. Mater. 2025, 3, 2234−2258

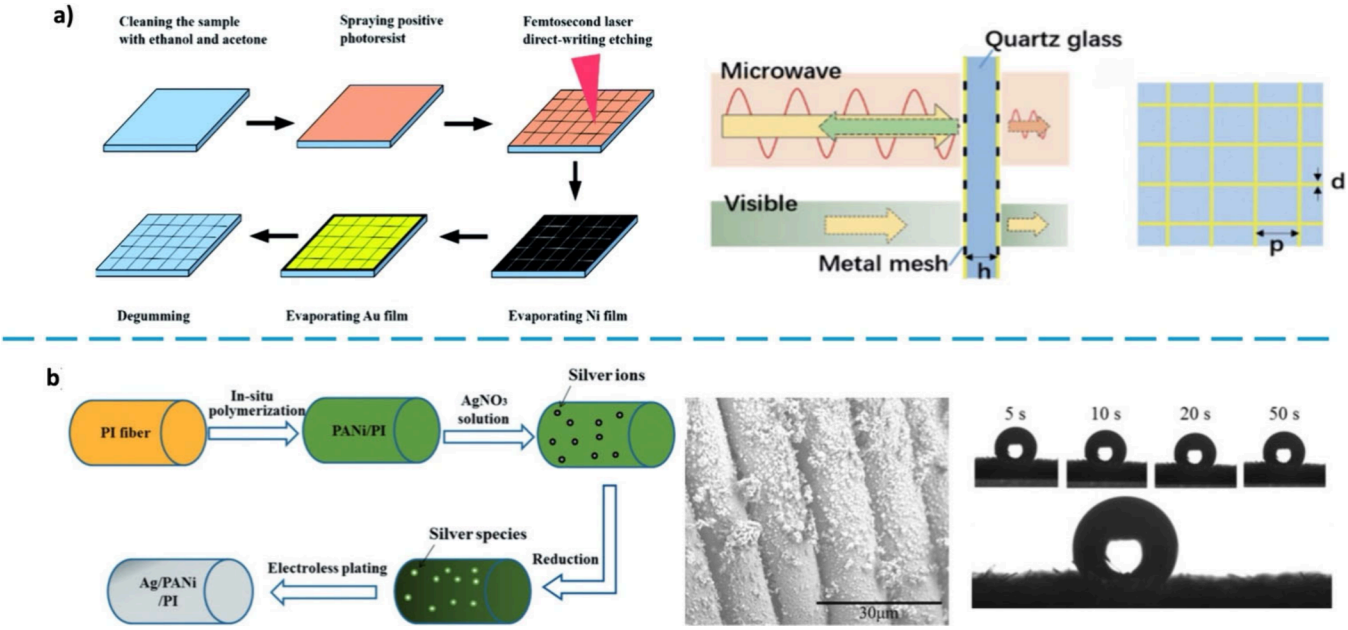

Figure 8. (a) The metal mesh manufacturing process for windows. [Modified from Zhang et al.[86] under the terms of the Creative Commons Attribution International License (CC BY)]. (b) The process of the preparation of Ag/PANi/PI fabric by PANi in situ reduction. [Reproduced with permission from ref 91. Copyright 2017 Sage Publications].

quality graphene films with excellent conductivity, though it can lead to surface damage due to thermal effects. Electrospinning produces ultrafine graphene fibers that yield films with high surface area and mechanical strength, but it requires careful management of solution viscosity and electric field strength. Each method has its specific applicability, and adjustments should be made based on application requirements considering scalability, cost, and material properties. Future research can focus on improving and optimizing these methods as well as integrating them to enhance the performance and applicability of graphene-based composite films.

Except for dense films, as an excellent electromagnetic shielding material, graphene advanced aerogel film is also widely studied. Achieving high performance and multifunctional integration is the core goal of the development of advanced aerogel film, and its leap-forward performance depends largely on the innovation of manufacturing process.[80] Among them, directional freeze-casting technology has become the core strategy for constructing ordered microstructures. Aerogels and hydrogels with specific oriented microstructures are constructed by controlling the growth direction of ice crystals, that is, using solvents (usually water) to solidify into ice crystals, solutes or suspended particles are squeezed between ice crystals, and then the ice crystals are sublimated by freeze-drying, leaving a porous structure opposite to the ice crystal template.[81,82]

This controlled anisotropic structure is crucial for optimizing material performance because it can build a continuous "highway" for electron or phonon transmission, thereby significantly improving the electromagnetic shielding effectiveness or thermal management capabilities of the material.[83] In recent years, researchers have further developed more complex freezing techniques based on traditional unidirectional freezing, and combined with the introduction of new nanomaterials (such as MXene, cellulose, etc.), they have achieved fine control of the pore structure and wall thickness, thereby constructing a composite aerogel with both ultrahigh strength and excellent functionality. These advanced manufacturing methods not only demonstrate excellent microstructure control capabilities, but also promote the rational design and development of the next generation of high-performance aerogel films with specific functions, showing great application potential.[84]

4. GRAPHENE COMPOSITE FILM AS EMI SHIELDING MATERIALS

Research has shown that the effectiveness of electromagnetic interference shielding is closely related to the material's inherent electrical conductivity or magnetic permeability. As a result, materials with high conductivity or magnetic permeability are widely used in EMI shielding applications. Currently, EMI shielding materials can be primarily categorized into two types: metallic materials and polymer materials.

4.1. Traditional Metallic Materials as EMI Shielding Materials

Traditional metallic materials can be classified into electromagnetic shielding materials, represented by silver, copper, and aluminum, and magnetic shielding materials, represented by iron, manganese alloys, and magnetic steels. Currently, electromagnetic shielding metals are typically chosen for their high electrical conductivity. However, pure metal materials are often limited in widespread application due to drawbacks such as heavy weight, lack of flexibility, high cost, susceptibility to corrosion, relatively simple properties, and difficulty in precise control of performance. To address these issues, some researchers have processed metals into mesh structures to reduce weight and enhance electromagnetic SE.[85,86] The metal mesh manufacturing process for window fabrication is shown in Figure 8a. Also, other studies have incorporated metals as conductive fillers, combining them with organic carbon materials (e.g., graphene and carbon nanotubes) or functional inorganic materials to form composite

https://doi.org/10.1021/acsaenm.5c00207
ACS Appl. Eng. Mater. 2025, 3, 2234−2258

materials,[87,88] further improving shielding performance and other properties.

4.2. Polymer-Based EMI Shielding Materials

The differences in the conductivity of polymers allow them to be classified into two main categories: intrinsic conductive polymers and nonconductive polymers. In the field of electromagnetic shielding, polymers are widely used due to their high plasticity, ease of processing, good chemical stability, and relatively low cost. For intrinsic conductive polymers, the conjugation within the molecular chains allows π-electrons to delocalize,[89] moving freely between multiple atoms rather than being confined to a single chemical bond.[90] This delocalization influences the material's dielectric constant and magnetic susceptibility, thereby enhancing the polymer's conductivity. To achieve higher electromagnetic shielding effectiveness, some researchers have also controlled the chemical structure by modifying the chemical composition.[91−93] Figure 8b shows the process of the preparation of Ag/PANi/PI fabric by polyaniline (PANi) in situ reduction; also the SEM and contact angle (CA) analysis photo are shown in this figure. For nonconductive polymers, it is typically necessary to incorporate conductive fillers to transform them into high-performance electromagnetic shielding materials. These materials primarily rely on electromagnetic absorption. Therefore, to enhance electromagnetic absorption performance, researchers have designed various unique structures, such as layer-by-layer assembly structure,[94,95] multilayer structure[96] and foam structure,[97,98] etc. Optimizing the electromagnetic shielding effectiveness by adjusting the type, morphology, volume fraction of fillers, as well as the properties of the polymer matrix is a primary research direction and a focus on current studies.

4.3. Graphene-Based Polymer Composites as EMI Shielding Materials

Research on inorganic nonmetallic materials as electromagnetic shielding materials has made significant progress in recent years. These materials typically exhibit excellent thermal stability,[99] chemical stability,[100] and good mechanical properties, making them more resistant to corrosion and stable over long periods in harsh environments, such as high temperatures and high humidity. Carbon-based materials, as key inorganic nonmetallic materials, offer high flexibility in design and performance control. By combining carbon-based fillers, such as carbon black,[101] carbon fibers,[102−104] carbon nanotubes (CNT),[105−109] with different matrix materials (e.g., rubber, thermoplastic materials), optimized composites can be developed to meet the wave-absorbing requirements across various frequency bands. Utilizing the porous[110] or multilayered structures[111] of inorganic nonmetallic materials, thin films, foams, aerogels, and hydrogels can be fabricated, which effectively enhance their electromagnetic wave absorption and reflection efficiency.

Graphene is a two-dimensional carbon allotrope composed of a single layer of sp^2 bonded carbon atoms, exhibiting exceptional mechanical properties (Young's modulus of approximately 1 TPa), high electrical conductivity (≈ 6000 S/cm), an extremely high specific surface area (2630 m^2/g), and excellent thermal conductivity (≈5000 W/m·K). However, pure graphene tends to have difficulty achieving uniform dispersion in polymers and is incompatible with organic polymers.[112] Therefore, the incorporation of graphene with other polymers has been considered an effective strategy. At lower concentrations, graphene can be used as a filler to easily combine with various thermoplastic (or thermosetting) polymers, forming polymer nanocomposites with remarkable physical, mechanical, and chemical properties.[113] Overall, graphene-based EMI shielding composite films can be divided into two categories: graphene-based metal composite films and graphene-based organic polymer composite films.

Before discussing the application of graphene as an electromagnetic shielding material, it is necessary to first explore a core challenge that limits its electrical performance: how to maintain high carrier mobility (e.g., >10,000 $cm^2/V{\cdot}s$) in large-area graphene films. Although graphene has extremely high intrinsic mobility in theory, in the large-area films actually prepared, there are inevitably grain boundaries and scattering from the substrate, which will seriously weaken its electrical performance.

The current research consensus and response strategies mainly focus on the following aspects:

a. Optimize the growth process to increase the crystal domain size: By optimizing CVD growth conditions (such as regulating growth temperature, gas flow rate and pressure), the formation of large-sized single-crystalline graphene domains can be promoted, thereby reducing the number of grain boundaries per unit area.[114] Furthermore, studies have shown that growth temperatures close to the melting point of copper can help reduce the surface roughness of the substrate and reduce nucleation sites, thereby obtaining graphene films with larger domains and fewer defects.[115]

b. Develop advanced lossless transfer technology: The traditional "etching-transfer" process easily introduces wrinkles, damage and chemical residues, which seriously affect the electrical properties of graphene. Therefore, academia and industry are actively developing milder and cleaner transfer technologies, such as electrochemical bubbling or dry transfer assisted by van der Waals forces, to maximize the integrity and cleanliness of graphene films.[116]

c. Exploring the weak interaction basis: Charge doping and phonon scattering of graphene by the substrate are also important factors limiting the mobility. The study shows that using an atomically flat insulating substrate such as hexagonal boron nitride (h-BN) that matches the graphene lattice can significantly attenuate substrate-induced scattering, thereby achieving high carrier mobility close to its intrinsic value in the transferred graphene.[117]

The introduction of graphene can significantly improve the mechanical properties of the polymer matrix, especially the fracture toughness and fatigue resistance. The dispersion quality and orientation state of the filler are key to determining the reinforcement effect. When it comes to the dispersion quality, good dispersion is crucial. Studies have shown that by uniformly dispersing only 0.5 wt % of graphene nanosheets in epoxy resin, the fracture toughness of the composite material can be increased by 40%.[118] The toughening mechanisms include crack deflection, crack bridging, and crack pinning effect induced by well-dispersed two-dimensional fillers, which can effectively dissipate the fracture energy.[119] On the contrary, filler agglomeration will become stress concentration points, which will weaken the mechanical properties of the material. As for orientation, although the precise quantification

https://doi.org/10.1021/acsaenm.5c00207
ACS Appl. Eng. Mater. 2025, 3, 2234−2258

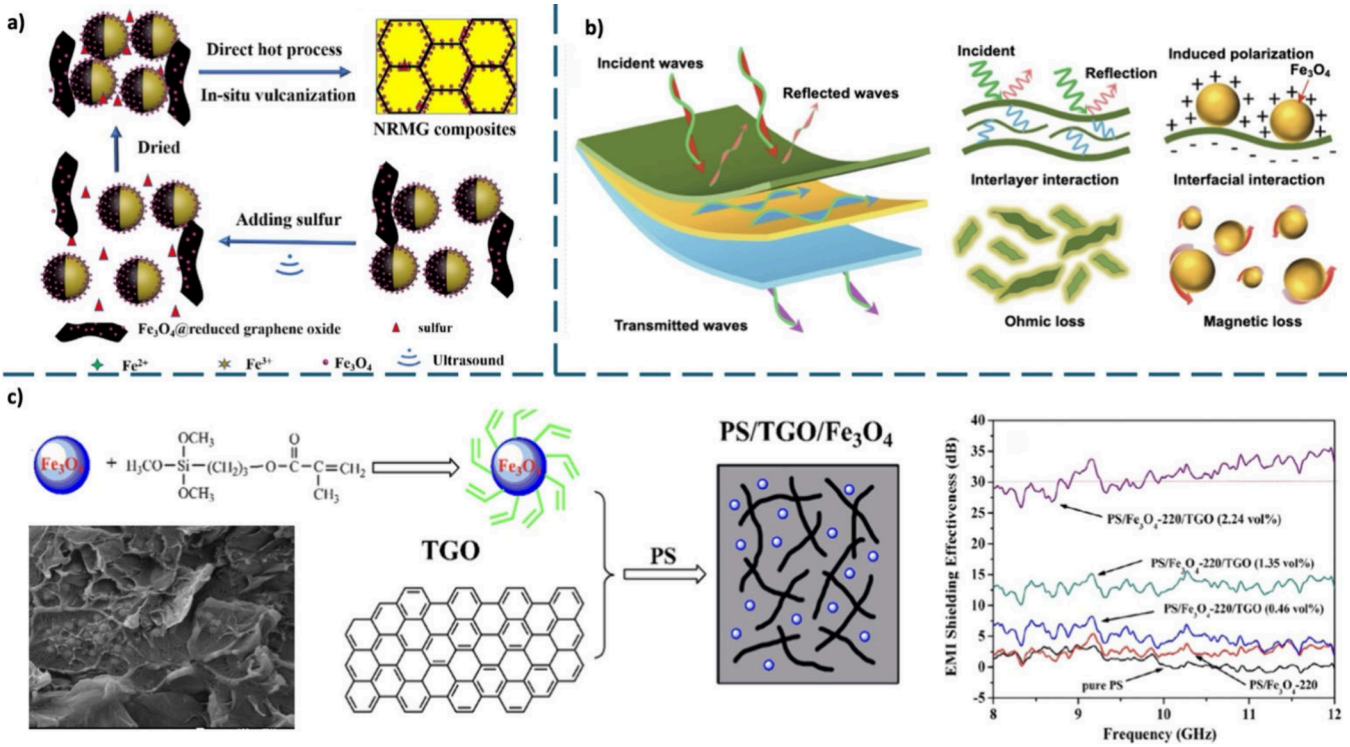

Figure 9. (a) Schematic illustration of the preparation process of the NRMG composites. [Reproduced with permission from ref 126. Copyright 2018 Elsevier, Ltd.]. (b) EMI shielding mechanism of the Fe_3O_4/PI composite films. [Modified from Guo et al.[127] under the terms of the Creative Commons Attribution International License (CC BY)]. (c) Schematic of the syntheses of PS/TGO/Fe_3O_4 composites and EMI SE with different loading of TGO. [Reproduced with permission from ref 128. Copyright 2014 Elsevier, Ltd.].

of the direct relationship between the orientation angle and mechanical properties is still a research hotspot, its positive impact has been widely confirmed. Oriented graphene sheets can more effectively hinder the initiation and propagation of microcracks. Studies have reported that adding a small amount (≤1 wt %) of well-oriented graphene oxide to epoxy resin can increase its tensile fatigue life by up to 1580%.[120]

4.3.1. Graphene-Based Metal Composite Films. As a matrix material, graphene possesses an extremely high specific surface area and excellent electrical conductivity, which effectively provide a pathway for electromagnetic wave attenuation. The incorporation of metal particles, i.e., Ni,[121−125] Fe_3O_4,[126−128] AgNWs,[129,130] AgNPs,[131] Cu,[132−134] Co,[135] FeNPs,[136] TiO_2,[58] ZnO,[137] further enhances the conductivity and EMI shielding performance of the composite material. Metal fillers not only improve the reflection and absorption capabilities of the composite material toward electromagnetic waves but also optimize the attenuation of electromagnetic waves by increasing the electrical conductivity and enhancing the interface effects within the composite.[138] The thickness of graphene-based composite films, the type and amount of metal particles employed, and the frequency range employed are key factors of interest for researchers in this field.

Fe_3O_4 can significantly improve the electron transfer efficiency. Zhan et al.[126] fabricated a segregated network structure of natural rubber/Fe_3O_4@rGO composite (NRMG) via a self-assembly method (Figure 9a). Compared to the pure natural rubber/rGO (NRG) composite, the EMI SE of the NRMG composite was 1.4 times higher, and it demonstrated excellent stability in the frequency range of 8.2−12.4 GHz. Even after 2000 bending-release cycles, the shielding performance decreased by only 3.5%. Guo et al.[127] developed hierarchically multifunctional polyimide (PI) composite films using a strategic design approach, incorporating a three-layer structure with distinct functions (Figure 9b). The top layer, composed of GO/expanded graphite (EG), serves as both a thermal conductor and an EMI shielding layer. The middle layer, Fe_3O_4/PI, enhances EMI SE, while the substrate layer, made of electrospun PI fibers, improves the mechanical properties. The composite films, containing 61.0 wt % GO/EG and 23.8 wt % Fe_3O_4/PI, exhibit high EMI SE (34.0 dB) and good tensile strength (93.6 MPa). Chen et al.[128] fabricated composite materials with enhanced EMI SE by incorporating thermally exfoliated reduced graphene oxide (TGO) and magnetic Fe_3O_4 nanoparticles into polystyrene (PS) (Figure 9c). They found that the PS/TGO/Fe_3O_4 composites exhibited significantly higher electrical conductivity and EMI SE compared to the PS/Fe_3O_4@RGO composites. Notably, the PS/TGO/Fe_3O_4 composite with 2.24% graphene content demonstrated an EMI SE of over 30 dB in the frequency range of 9.8−12 GHz.

Nickel-doped graphene composite films have also attracted significant attention from many researchers. Yan et al.[122] developed a novel composite phase change material (PCM) based on a dual-network structure of lignin carbon aerogel and nickel foam, aimed at achieving multisource energy harvesting and EMI shielding. The PEG/Ni−F/LN-rGO (PLGN) composite material was synthesized by vacuum-assisted impregnation of poly(ethylene glycol) (PEG) into a nickel foam/lignin/rGO scaffold. The resulting PLGN composite exhibited excellent electrical conductivity (1597.5 S/cm) and significant photo- and electrothermal conversion capabilities. The EMI shielding effectiveness of PLGN reached 69.9 dB in X-band (Figure 10a). Also, Liang et al.[124] designed flexible

https://doi.org/10.1021/acsaenm.5c00207
ACS Appl. Eng. Mater. 2025, 3, 2234−2258

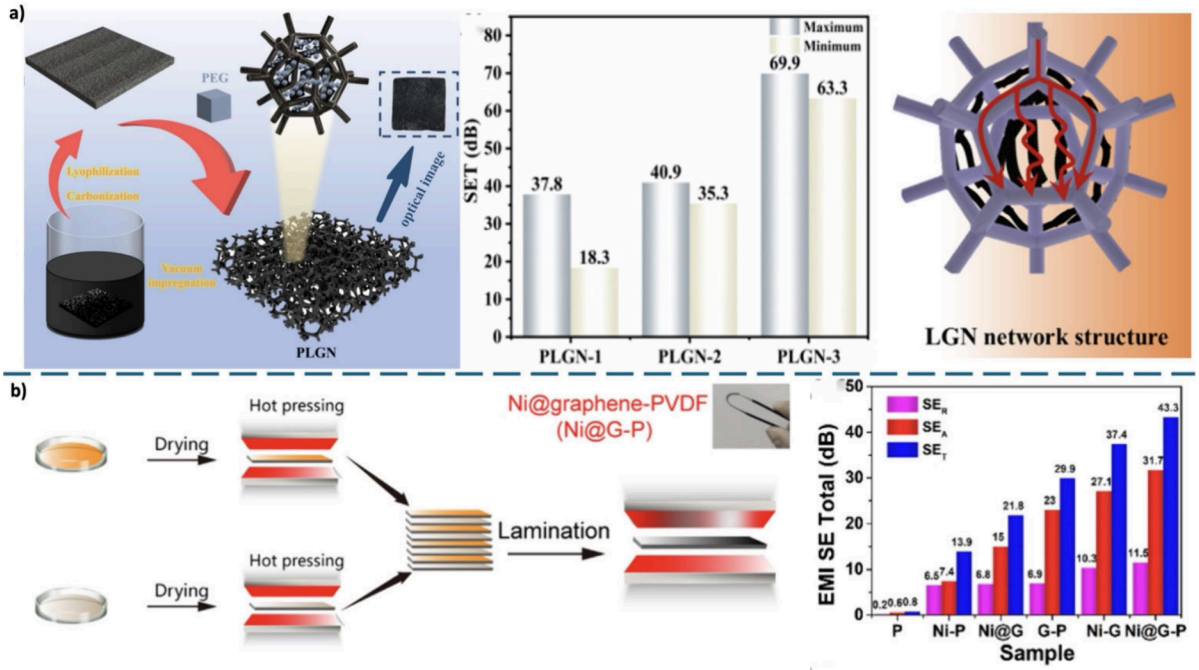

Figure 10. (a) PLGNs with a superb EMI SE [Reproduced with permission from ref 122. Copyright 2024 Elsevier, Ltd.]. (b) Ni@G-P films for EMI and thermal management. [Reproduced with permission from ref 124. Copyright 2020 Elsevier, Ltd.].

Table 2. EMI SE and Electrical Properties of Graphene-Based Metal Composite Films

Filler	Matrix	Synthesis method	Conductivity range	SE_T (dB)	Frequency Range	ref.
$NiFe_2O_4$	NFO-Gx (x represents different graphene content	Crystallization−Ultrasound treatment−Annealing	Increase with the graphene content (NFO-G_3 reaches highest)	26.5−40.6	2−18 Ghz	121
Nickel foam	PLGN	Vacuum-assisted impregnation	1597.5 S/cm (PLGN-3)	37.8−69.9	X-band	122
$NiFe_2O_4$	NFO-G	Hydrothermal process−Heat treatment	~	15−23	2−18 GHz	123
Ni-G	HAMS	Stacking hot pressing technique	1.6−76.8 S/m	21.8−51.4	X-band and Ku-band	124
$Ni_{0.5}Co_{0.5}Fe_2O_4$	RGO	One-pot synthesis−Hydrazine hydrate and calcination	~	9.1−36.3	12.4−18 GHz	125
Fe_3O_4	NRMG	Self-assembly and compression molding	6.1 S/m (NRMG-10)	28.6−32.1	X-band	126
Fe_3O_4/PI	GO/EG	Hierarchical design and assembly	230.0 S/cm (61.0 wt % GO/EG)	23.8−34.0	X-band	127
PS/Fe_3O_4	TGO	Blending of PS with TGO and modified Fe_3O_4 nanoparticles	21 S/m (2.24% of graphene)	25−36	9.8−12 GHz	128
AgNWs	RGO/AgNWs hybrid aerogels	Reduction- Freezing and ambient-pressure drying	\	17.1−45.2	X-band and Ku-band	129
AgNWs	GO	Two-step spin-coating		28−40.1	Ku-band and K-band	130
AgNPs	Ag/Graphene hybrid	Ammonium sulfate electrolyte-Vacuum filtration	\	8−29.9	8−12 GHz	131
Cobalt nanoparticles	GO	Soaking- Immersion in graphene oxide- Carbonized	217 S/m (Silk Cocoon-Cobalt-Graphene-0.9)	27−55	Ku-band	135
Fe_3O_4 nanoparticles and carbon fiber	RGO	Mixing- Thermal reduction under vacuum	~	22.18 (10.64 GHz for a thickness of 2 mm.)	9.2−12.32 GHz	136
TiO_2−$Ti_3C_2T_X$	GF	Vacuum assisted filtration-Pyrolysis under argon	Surface resistance is 7.5 Ω/sq	18−27 (12.4 GHz)	2−18 GHz	58
ZnO nanopowder	graphene nanoplatelets	Hydrothermal method-Brush coating	~	30−38	10−20 GHz	137

poly(vinylidene fluoride) (PVDF) composite films with an alternating multilayer structure (HAMS), incorporating highly aligned graphene nanosheets and nickel nanowires. The composite films exhibited enhanced electrical conductivity, with the optimal HAMS film showing a conductivity of 76.8 S/m, and demonstrated excellent EMI SE of up to 51.4 dB (Figure 10b). The films also exhibited a significantly improved in-plane thermal conductivity of 8.96 W/m·K. The graphene-based metal composite films are summarized in Table 2.

4.3.2. Graphene-Based Organic Polymer Composite Films. The composite of graphene and organic polymers can significantly improve the flexibility and stability of the material, allowing it to have huge potential in flexible electronic devices, smart materials, and other high-performance application

https://doi.org/10.1021/acsaenm.5c00207
ACS Appl. Eng. Mater. 2025, 3, 2234−2258

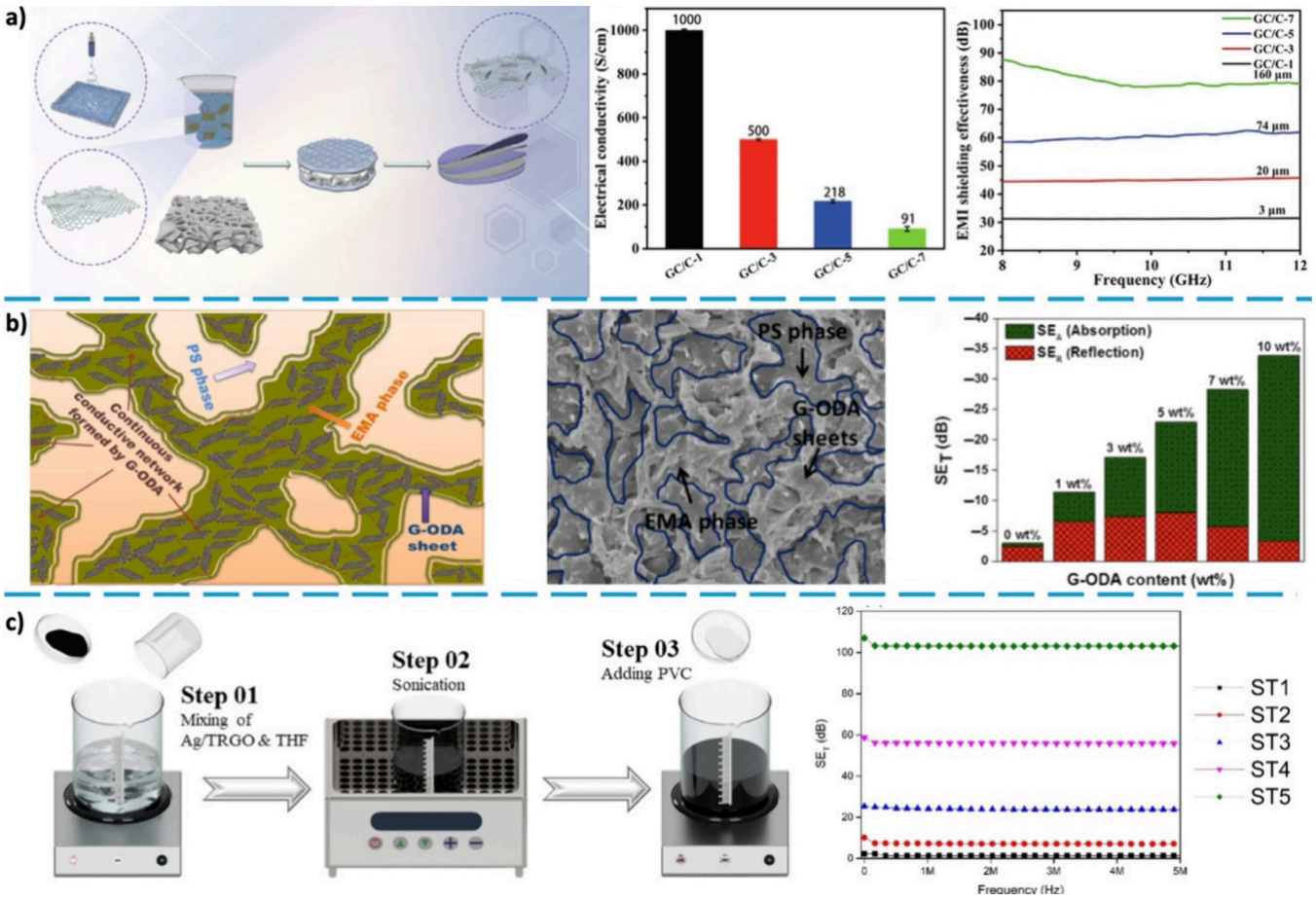

Figure 11. (a) Porous alternating PVA-derived carbon and graphene layers composite. [Modified from Li et al.[145] under the terms of the Creative Commons Attribution International License (CC BY)]. (b) PS and EMA composites with high EMI SE. [Modified from Ghosh et al.[149] under the terms of the Creative Commons Attribution International License (CC BY)]. (c) Nanosilver-Decorated Graphene/PVC nanocomposite films. [Reproduced with permission from ref 152. Copyright 2023 Elsevier, Ltd.].

products. The main graphene-based polymeric organic materials are as follows: PVA,[139−145] PS,[146−149] poly(vinyl chloride) (PVC),[150−152] polyurethane (PU),[42,153,154] epoxy (EP),[155−158] polypropylene (PP).[159,160]

PVA was usually utilized as a polymer for EMI shielding with graphene. Li et al.[145] fabricated a multilayer film consisting of alternating layers of PVA-derived carbon and graphene using a vacuum-assisted filtration method. The film has a total thickness of 160 μm and consists of seven alternating layers, achieving an EMI SE of 80 dB in the X-band. The film exhibits a tensile strength of up to 16 MPa and maintains stable electrical conductivity (up to 117 S/cm) after 250 bending cycles (Figure 11a). PS was also a main kind polymer used for EMI shielding, Ghosh et al.[149] fabricated thermoplastic elastomeric blend composite films made from PS and ethylene-*co*-methyl acrylate (EMA) using a solution mixing method, incorporating amine-functionalized reduced graphene oxide (G-ODA) as a filler. By selectively localizing G-ODA in the EMA phase, they created an interconnected conductive network, significantly reducing the electrical percolation threshold. The composite films achieved an electrical conductivity of 0.9 S/cm and a thermal conductivity of 0.95 W/m·K with 10 wt % G-ODA loading. The films demonstrated an EMI SE of 35 dB in the X-band frequency range. PVC substrate has also attracted widespread attention from researchers due to its strong adjustability (Figure 11b). Shahzad et al.[152] used a solution casting method to incorporate varying concentrations of Ag/TRGO nanoparticles into PVC nanocomposite films. The films with 50 wt % Ag/TRGO exhibited the highest Alternating Current conductivity (6.23×10^2 S/cm). These films demonstrated an EMI SE exceeding 100 dB in the frequency range of 100 Hz to 5 MHz and showed almost no transmission of near-infrared (NIR) radiation (Figure 11c).

Feng et al.[42] successfully developed a graphene/CNT/PU composite film through a scalable production method, featuring a dense three-dimensional multilayer structure. The composite film exhibits a tensile strength of 42.9 MPa and a conductivity of 2087.2 S/m. Its EMI SE reaches 37.7 dB at a thickness of 130 μm and can reach up to 72.1 dB at a thickness of 520 μm. The fabrication progress and relevant value of the EMI SE are shown in Figure 12a. Additionally, the GC/PU film demonstrates excellent electric heating performance (with a surface temperature of 127.5 °C at 5.0 V and a thermal response time of less than 20 s) and flame-retardant capabilities, making it suitable for applications such as anti-icing and deicing. Epoxy, with its strong corrosion resistance, ease of processing, and nontoxicity, is also used as a high-performance composite material.

Wang et al.[157] proposed a low-cost, lyophilization-free method to fabricate graphene aerogel films with long-range oriented structures. By combining thermochemical reduction

https://doi.org/10.1021/acsaenm.5c00207
ACS Appl. Eng. Mater. 2025, 3, 2234−2258

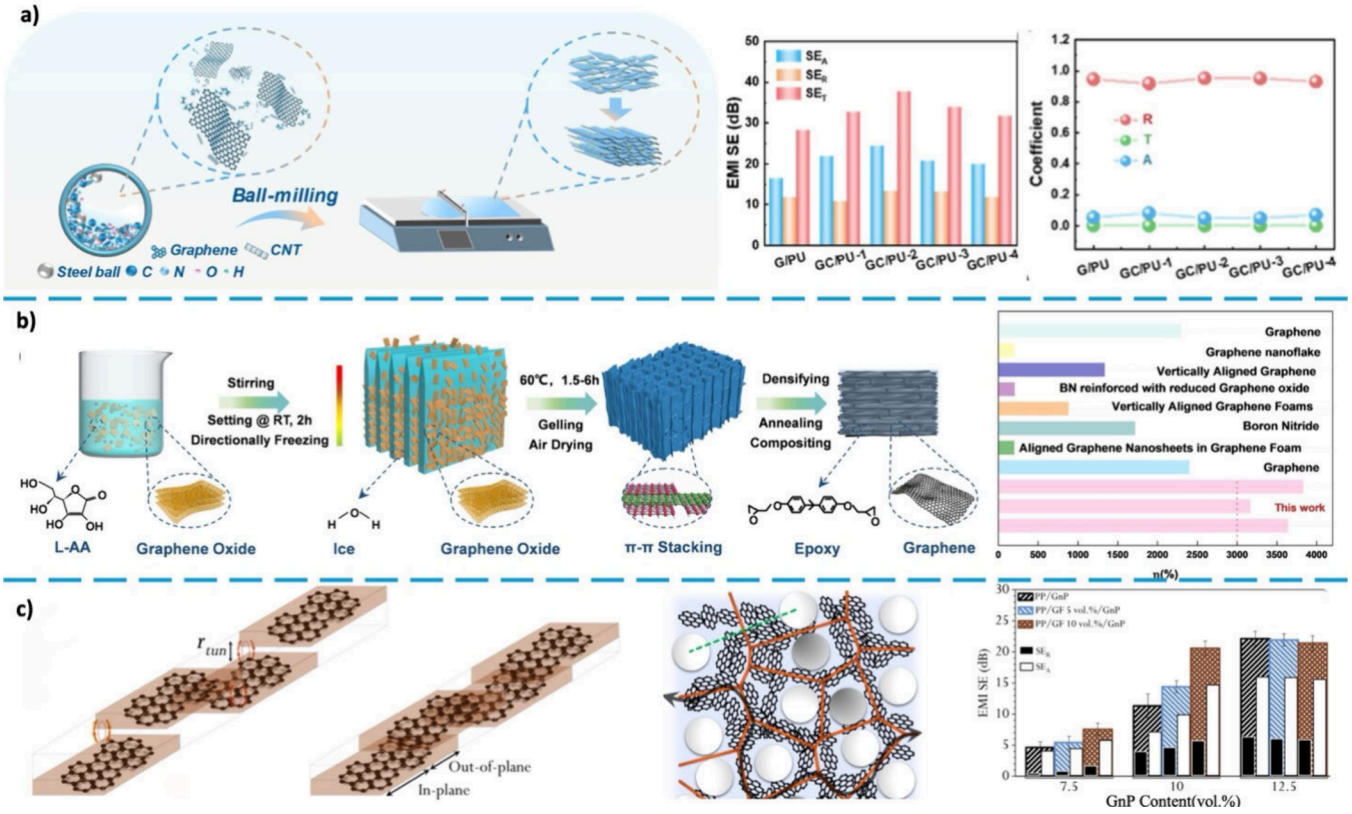

Figure 12. (a) Flexible GC/PU film. [Reproduced with permission from ref 42. Copyright 2024 Elsevier, Ltd.]. (b) Multifunctional properties of epoxy-graphene composite films. [Reproduced with permission from ref 157. Copyright 2023 Elsevier, Ltd.]. (c) PP-based composite with graphene nanoplatelets (GNPs) coated on the GFs. [Reproduced with permission from ref 159. Copyright 2023 Elsevier, Ltd.]

Table 3. EMI SE and Electrical Properties of Graphene-Based Organic Polymer Composite Films

Filler	Matrix	Synthesis method	Conductivity range	SE_T (dB)	Frequency Range	ref.
PVA	Few-layered graphene (FLG)	Mixing-Simple casting	0.5S/cm (0.5 vol %FLG)	~12.5 (0.1 vol %FLG) ~19.5 (0.5 vol %FLG)	X-band	142
PVA/polypyrrole	Graphene quantum dots (GODs)	Solvent casting method	~	2.2−9.8 (8−12 GHz) 2.1−8.9 (12−20 GHz)	8−20 GHz	143
PVA/TiO_2	RGO	Casting-Drying	~	3.73−31.34	X-band	144
PVA	Graphene/Carbon multilayer film (GC/C)	Vacuum-assisted filtration-Carbonization	997 S/cm (GC/C-1) 117 S/cm (GC/C-7)	32−80	X-band	145
PANI/PS	GO	Casting method	0.000326 S/cm (1.5 wt % GO)	36.87−40.11	X-band	148
PS/EMA	G-ODA	Mixing-Compression molding	0.9 S/cm (10 wt % G-ODA)	17−35	X-band	149
PVC/wood plastic	GNP	Blending-Hot pressed method	~	3.64−25.81	8−9 GHz	150
PVC/Fe_3O_4	Graphene	Solution mixing method	0.00077 S/m	8.5−13	X-band	151
Thermoplastic polyurethane (TPU)	RGO	In-situ reduction method-supercritical CO_2 foaming	2.77 S/m (3.71 vol % RGO)	20−24.7 (3.71 vol % RGO)	X-band	154
PU	Graphene/CNT (GC)	Liquid-phase ball milling-Coating	817.7−2087.2 S/m	37.7−72.1 (GC/PU-2)	X-band	42
EP	Aligned graphene	Lyophilization-free "fire-and-ice" method	170−830 S/m	41−47.5	10−15 GHz	157
EP/polypyrrole (PPy)/ magnetite nanoparticles (MP)	GO/Carbon fiber	PPy coating-GO/MP synthesis-Vacuum mixing	5.75 × 10^{-8} S/m (0.2% GO with 0.2% MP)	46.72−50 (0.2% GO with 0.2% MP)	X-band	158
PP	GNP/GF	Dry blending technique-Injection molding	0.16 S/m (PPGNP12.5GF10)	19−20.56 (10 vol % GNP and 10 vol % GF)	Ku-band	159
Micropoder PP	RGO/Multiwalled carbon nanotubes (MWCNTs)	Ammonia solution and pyrogallol-Hot pressed method	0.0295 S/m (5% MWCNTs and 0.5% GO)	15.6−16 (mPP/RGO/ MWCNTs-5)	X-band	160

and directional freezing, they successfully produced graphene/EP composites. The composite, with only 1.84 vol % graphene content, exhibited an ultrahigh thermal conductivity of approximately 11.6 W/m·K, achieving an enhancement efficiency of 3640% compared to the matrix material (Figure 12b). The compressive strength of the composite increased by

https://doi.org/10.1021/acsaenm.5c00207
ACS Appl. Eng. Mater. 2025, 3, 2234−2258

2.6 times, while the modulus remained low, demonstrating excellent deformability. Additionally, the composite showed high electrical conductivity and significant EMI SE (~40 dB), indicating its broad potential for use as thermal interface materials (TIMs) and EMI shielding in advanced electronic packaging applications. PP, with its good heat resistance and low density, has recently been studied for composite applications with graphene. Salari et al.[159] developed a hybrid material with enhanced multifunctional properties by incorporating graphene nanoplatelets (GNPs) and glass fibers (GFs) into a PP-based composite. By controlling the arrangement and orientation of the fillers, these hybrid composites exhibited a six-order magnitude improvement in electrical conductivity, a 723% increase in real permittivity, and demonstrated an EMI SE of 20.56 dB in the Ku-band (Figure 12c). Furthermore, the thermal conductivity of the hybrid composites increased from 0.67 to 1.09 W/m·K, while the tensile strength improved by 109%. Table 3 shows some main graphene-based organic polymer composite films.

The future development will focus on the application of multifunctional graphene-based composite films. As various novel organic polymers, such as polydimethylsiloxane (PDMS), poly(ether imide) (PEI), poly(phenylene-carborane) (PPB), poly(ether-*block*-amide) (PEBAX), unsaturated polyester (UPES), and polyvinylpyrrolidone (PVP), are increasingly considered for the fabrication of graphene-based polymer composite films, research will deepen the understanding of the performance and application requirements of these composite materials. Future research and development will aim to enhance their stability and sustainability under extreme conditions, driving their widespread application in industries such as aerospace, electronics, and automotive.

4.4. Graphene Preparation Strategies: Advantages and Disadvantages of Top-down and Bottom-up Approaches

From the perspective of graphene film synthesis strategy, the "top-down" and "bottom-up" paths show their own unique advantages and limitations. As the name suggests, the bottom-up strategy starts from the atomic or molecular level and gradually builds up the structure of graphene through chemical reactions or precise assembly processes.[161] This usually results in high-quality, defect-free, and structurally controllable graphene or graphene nanoribbons. The top-down strategy starts from a larger bulk material (usually graphite) and exfoliates, cuts or reduces it through physical or chemical means to obtain graphene.[162] The two approaches present significant differences in scalability, defect density, and the electronic properties of the resulting materials, which directly determine their applicability in different application scenarios.[163,164]

Top-down strategies represented by mechanical exfoliation can obtain atomically perfect graphene with few defects.[165] Its excellent conductivity comes from an extremely high carrier mobility and low scattering. This high-quality graphene can theoretically provide excellent electromagnetic shielding performance, but due to its extremely limited production and size constraints, it is difficult to meet the needs of large-area continuous films in practical applications. On the contrary, although bottom-up strategies such as CVD can achieve large-area, controllable number of graphene preparation,[166] its products usually have structural defects such as grain boundaries and vacancies, and the additional damage that may be introduced during the transfer process will reduce its intrinsic conductivity. Nevertheless, for applications in electromagnetic shielding that emphasize the continuity and high conductivity of the macroscopic conductive network of materials, CVD graphene, with its excellent scalability, makes it possible to compensate for the effects of single-layer defects by stacking multilayer graphene or constructing composite materials.[167] With the advantage of large-area preparation, even if the shielding performance of single-layer graphene is slightly affected by defects, by optimizing the number of layers, film thickness and composite structure, CVD graphene can still show great application potential in the field of large-scale, low-cost electromagnetic shielding materials.[130]

5. A REVIEW OF THE TRENDING ARTICLES FROM THE PAST DECADE

To investigate the outstanding potential of various graphene-based composite films in the field of electromagnetic shielding, this study collected 40 high-citation articles published between 2014 and 2024. A three-dimensional surface plot, as shown in Figure 13a, was created with SE_R, SE_A, and conductivity as the

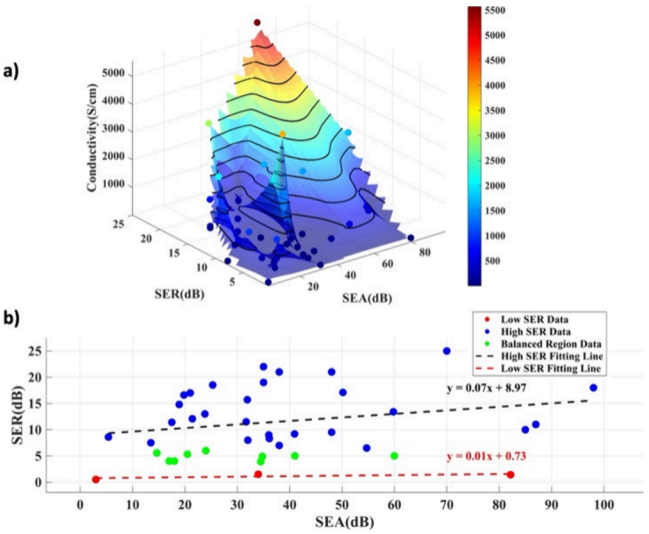

Figure 13. (a) SE_A-SE_R scatter plot. (b) SE_A-SE_R-Conductivity three-dimensional surface plot.

coordinates. Overall, most research focuses on materials in the X-band, and the SE_A values of these materials are generally higher than their corresponding SE_R values. Hwang et al.[168] proposed that EMI shielding materials dominated by absorption should have an absorption-to-incidence energy ratio (A) greater than 0.5, which corresponds to a SE_R value less than 3.01 dB. Using this standard, a low SE_R threshold of 3.01 dB was set, and SE_R values below this threshold were considered low SE_R data, while those above were categorized as high SE_R data. To further refine the classification, the SE_R data set was divided into three regions, with SE_R values greater than twice the threshold considered high SE_R, values between the threshold and twice the threshold as balanced, and those below the threshold as low SE_R. To explore the relationship between SE_A and SE_R in electromagnetic shielding materials, linear regression analysis was conducted separately on the data from the high SE_R and low SE_R regions, in order to better understand the differences in SE_R and SE_R behaviors across different SE_R ranges. As shown in Figure 13b, the regression

https://doi.org/10.1021/acsaenm.5c00207
ACS Appl. Eng. Mater. 2025, 3, 2234−2258

Table 4. Comparison of EMI Shielding Performance of Different Materials[a]

Materials name	SE_A (dB)	SE_R (dB)	Frequency range	Conductivity (S/cm)	ref.
GF-2000	13.5	7.5	X-band	∼1000	40
G-E films	5.4	8.6	X-band	2.5	169
PCNT/MWCNT	87	11	Ku-band	29.5	170
Graphitized r-GO/SiO_2	21	17	X-band	0.0137	171
PS/TGO/Fe_3O_4	24	6	X-band	0.21	128
rLGO	14.65	5.55	1 GHz	243	172
MWCNT/WPU	38	7	X-band	0.45	173
$Ti_3C_2T_x$/SA	35	22	X-band	2963	20
Microcellular G-foam	32	8	X-band	3.1	174
$Ti_3C_2T_x$@PS-570	54.7	6.5	X-band	10.81	175
hydrophobic Mxene	60	5	X-band	580	176
GF/PEDOT: PSS-4.6	85	10	X-band	35.2	177
CNT/MLGEP/PDMS	34.5	3.9	X-band	0.55	178
d-$Ti_3C_2T_X$/CNF	20.5	5.3	Ku-band	1.155	179
MXene/SWCNT	3	0.5	X-band	130	180
CNTs/Ti_3C_2 MXene	31.9	15.7	X-band	238.12	181
$Ti_3C_2T_X$ MXene (350°)	98	18	X-band	1750	182
Ag/FeCo@rGO	82.2	1.4	X-band	3.039	183
MXene/$AgNW_{948}$−PVA	19.8	16.6	X-band	131	184
AgNWs/cellulose	70	25	X-band	5571	185
Ni@G-P	31.7	11.5	X-band	0.768	124
rGMH-5/epoxy	48	21	X-band	3.871	186
PG/PI	25.3	18.5	X-band	780	187
Fe_3O_4@rGO/MWCNT	34	1.5	X-band	11.458	188
MX-rGO	34.8	4.9	X-band	10	189
FC-ANF/CNT	48	9.5	X-band	2.3	190
Flame-retardant PVA/MXene	36.1	8.3	X-band	7.16	191
$Ti_3C_2T_X$/rGO	38	21	X-band	380	192
NFC/Fe_3O_4-5&CNT/PEO-4	17.5	11.4	X-band	39	193
rG-M	35	19	X-band	74.4	194
Fe_3O_4/PI	23.8	13	X-band	230	127
CNF/AgNW	50.17	17.09	X-band	1673	195
rGH@FeNi/epoxy	41	5	X-band	0.387	196
rGO/AgNW	18.9	14.8	X-band	2120	197
FGQF	36	9	X-band	3906	198
PVDF/MWCNT/GnPs	21.42	12.07	Ku-band	3.5×10^{-8}	199
LMHA/HCFG	59.8	13.4	X-band	1625.8	200
G-foams (PEG 20000)	17	4	X-band	0.0294	201
3D porous GnP30@PDMS	40.93	9.2	X-band	4.17×10^{-3}	202
MG-P13	18	4	X-band	∼1000	203

[a]G-E, multilayer graphene/ethylene-vinyl acetate copolymers; PCNT, Polymer Carbon Nanotube; rLGO, reduced Laser-induced Graphene Oxide; WPU, Waterborne Polyurethane; SA, Sodium Alginate; PEDOT:PSS, Poly(3,4-ethylenedioxythiophene) polystyrenesulfonate; MLGEP, Multilayer Graphene/Expanded Polystyrene; d-$Ti_3C_2T_X$, delaminated $Ti_3C_2T_X$; SWCNT, Single-Walled Carbon Nanotube; Ni@G-P, Ni@Graphene- Poly(vinylidene fluoride); rGMH, reduced Graphene Oxide-MXene; PG, Pristine Graphene; MX-rGO, Mxene-reduced Graphene Oxide; FC-ANF/CNT, Fluorocarbon-Aramid Nanofiber/Carbon Nanotube; NFC, Nanofibrillated Cellulose; PEO, Poly(ethylene oxide); rG-M, reduced Graphene oxide-MXene; rGH, regular honeycomb structure; FGQF, Ferromagnetic Graphene Quartz Fabric; HCFG, Hollow Carbon Fiber Grephene; LMHA, Ti_3CNT_X /HCFG/AgNW layered film; MG-P, Magnetic Graphene.

equation for the high SE_R region is $y = 0.067317x + 8.9725$, while for the low SE_R region, it is $y = 0.010198x + 0.72814$.

Meanwhile, we applied the K-means clustering method to analyze the three-dimensional data of the materials. Each cluster contains data points that are similar within the feature space. It optimizes the cluster centers iteratively, maximizing the similarity within clusters and minimizing the differences between clusters. K-means clustering does not rely on any prior labels, enabling the automatic identification of dense regions in the data based on its natural distribution, which is useful for uncovering inherent patterns within the data. In the analysis of materials based on SE_A, SE_R, and electrical conductivity, K-means clustering helped us categorize the materials into distinct clusters based on their SE_A, SE_R, and electrical conductivity characteristics, thereby identifying materials with higher similarity. The final clustering results are shown in Table 4.

At smaller values of k (such as $k = 3$ and $k = 7$), the range of the largest clustering region in SE_A, SE_R, and conductivity is relatively broad. With further increases in k to 11 and 15, the clustering region becomes more concentrated, and the distributions of absorption loss, reflection loss, and electrical conductivity become more focused. Between $k = 19$ and $k = 27$, the clustering region progressively narrows, and the differences in material characteristics become more pronounced. At $k = 27$, the SE_A range is from 36.1 to 41 dB, the SE_R range is from 5 to 9.2 dB, and the conductivity range is from 0.00417 to 7.16 S/cm. This indicates that as the value of k increases, the clustering method can better reflect the subtle differences in materials across the dimensions of SE_A, SE_R, and conductivity. Comparing the data in Table 4 with those in Table 5, it is observed that composite films primarily based on carbon nanotube structures, such as MWCNT/WPU, Fe_3O_4@rGO/MWCNT, and CNT/MLGEP/PDMS, exhibit significant characteristics and are likely to show potential in more fields in the future.

The research on graphene-based electromagnetic shielding materials has matured, $Ti_3C_2T_x$ Emerging two-dimensional

Table 5. Clustering Results of Materials Based on SE_A, SE_R, and Electrical Conductivity Characteristics

Value of k	SE_A range (dB)	SE_R range (dB)	Conductivity range (S/cm)
3	3−87	0.5−21	3.5×10^{-8}−1000
7	5.4−87	1.4−21	3.5×10^{-8}−74.4
11	5.4−87	1.4−21	3.5×10^{-8}−74.4
15	31.7−54.7	1.5−21	0.00417−11.458
19	17−38	1.5−17	3.5×10^{-8}−11.458
23	31.7−41	1.5−11.5	0.00417−11.458
27	36.1−41	5−9.2	0.00417−7.16
31	38−41	5−9.2	0.00417−0.45

https://doi.org/10.1021/acsaenm.5c00207
ACS Appl. Eng. Mater. 2025, 3, 2234−2258

materials represented by MXene have attracted much attention due to their unique advantages. Although MXene and graphene both have excellent metallic-level conductivity and two-dimensional layered structure, which provide a basis for building an efficient shielding network, there are key differences in their shielding mechanisms. Graphene-based materials (especially highly reduced graphene oxide) mainly rely on high conductivity to achieve reflection-dominated shielding, which may cause secondary electromagnetic pollution. In contrast, the core advantage of MXene lies in its "absorption-dominated" shielding mechanism.[204−206] The rich functional groups (−O, −OH, −F) on its surface not only give the material excellent water-phase dispersibility and simplify the processing process, but more importantly, these functional groups act as natural polarization centers, synergizing with the rich interfaces between MXene layers to produce significant dielectric losses through strong dipole polarization and interfacial polarization, thereby efficiently absorbing and dissipating electromagnetic wave energy.[20] However, MXene is easily oxidized in oxygen- and water-containing environments, resulting in performance degradation, which is the main bottleneck in its application. Graphene has excellent chemical stability and intrinsic mechanical properties, and its preparation technology is more mature. Therefore, the two are not substitutes but rather complementary in function: MXene is suitable for scenarios with high requirements for absorption performance and aqueous phase processing, while graphene has more advantages in fields that pursue long-term stability and structural strength (such as aerospace coatings). Designing graphene-MXene heterostructures and synergizing the advantages of both is an important direction to achieve performance excellence.[207,208]

In addition to MXene, the exploration of new electromagnetic shielding materials is developing in multiple dimensions toward the goal of "lightweight, ultrathin, broadband, and strong absorption". As a semiconductor two-dimensional material, transition metal sulfides (TMDs, such as MoS_2) focus on the dielectric loss caused by the band structure, crystal defects and heterogeneous interfaces, and are usually used as composite components to regulate the dielectric constant.[209,210] Porous carbon-based composites derived from metal−organic frameworks (MOFs) have shown great potential. They generate nitrogen-doped porous carbon skeletons embedded with metal nanoparticles (such as Co and Ni) in situ through high-temperature carbonization. This structure achieves absorption-dominated lightweight and efficient shielding through the synergistic effect of multiple mechanisms such as multiple internal reflections, conductive losses, magnetic losses, and strong interface polarization, but its preparation process is relatively complex and its mechanical properties are weak.[211]

6. CONCLUSION AND OUTLOOK

This review provides a comprehensive overview of the research progress on graphene-based composite films for EMI shielding. Early studies primarily focused on enhancing the fundamental properties of graphene composite films and investigating their composite effects on polymers and nanomaterials. Extensive research has been conducted on the advantages of graphene composite films in terms of electrical conductivity, flexibility, and thermal conductivity, particularly for applications in flexible electronic devices and portable hardware. As the research progressed, the focus of graphene composite films shifted toward functional improvements and large-scale applications, particularly in energy storage, sensors, and flexible electronics. Through various preparation methods, such as evaporation-induced self-assembly, vacuum filtration, doctor blade coating, and spin coating, the EMI shielding effectiveness of graphene composite films has been continuously improved, showing excellent absorption and reflection capabilities, especially in high-frequency applications.

Looking ahead, graphene-based composite films hold immense potential in the fields of smart materials and high-performance engineering plastics. As environmental issues become increasingly pressing, their application in green technologies, including energy storage, pollutant adsorption, and water treatment, has become a hot research topic. To further enhance the performance of these composite films, future research will focus on exploring more underdeveloped heteroatoms or novel polymers and their combinations to create more functionalized materials. Moreover, the integration of machine learning, multiscale simulations, and in situ characterization techniques, combined with existing polymer doping technologies, could significantly accelerate the development of next-generation graphene-based composite films and promote their applications in increasingly complex and demanding environments.

AUTHOR INFORMATION

Corresponding Authors

Zuhao Shi − *School of Physics and Mechanics, Wuhan University of Technology, Wuhan 430070, China; Hubei Engineering Research Center of RF-Microwave Technology and Application, School of Physics and Mechanics, Wuhan University of Technology, Wuhan 430070, China*; Email: zuhao17@whut.edu.cn

Daping He − *School of Physics and Mechanics, Wuhan University of Technology, Wuhan 430070, China; Hubei Engineering Research Center of RF-Microwave Technology and Application, School of Physics and Mechanics, Wuhan University of Technology, Wuhan 430070, China*; orcid.org/0000-0002-0284-4990; Email: hedaping@whut.edu.cn

Author

Daiyang Jiang − *School of Physics and Mechanics, Wuhan University of Technology, Wuhan 430070, China*; orcid.org/0009-0007-9185-7016

Complete contact information is available at: https://pubs.acs.org/10.1021/acsaenm.5c00207

Author Contributions

The manuscript was written through contributions of all authors. All authors have given approval to the final version of the manuscript.

Notes

The authors declare no competing financial interest.

ACKNOWLEDGMENTS

The authors acknowledge financial support from the National Natural Science Foundation of China (51672204, 51701146) and Foundation of the National Key Laboratory of Microwave Imaging Technology supported by the Fundamental Research Funds for the Central Universities (WUT: 2024IVA031).

https://doi.org/10.1021/acsaenm.5c00207
ACS Appl. Eng. Mater. 2025, 3, 2234−2258

REFERENCES

(1) Wang, X.-Y.; Liao, S.-Y.; Wan, Y.-J.; Zhu, P.-L.; Hu, Y.-G.; Zhao, T.; Sun, R.; Wong, C.-P. Electromagnetic Interference Shielding Materials: Recent Progress, Structure Design, and Future Perspective. *J. Mater. Chem. C* **2021**, *10* (1), 44−72.

(2) Redlarski, G.; Lewczuk, B.; Żak, A.; Koncicki, A.; Krawczuk, M.; Piechocki, J.; Jakubiuk, K.; Tojza, P.; Jaworski, J.; Ambroziak, D.; Skarbek, Ł.; Gradolewski, D. The Influence of Electromagnetic Pollution on Living Organisms: Historical Trends and Forecasting Changes. *BioMed. Res. Int.* **2015**, *2015*, 1−18.

(3) Schuermann, D.; Mevissen, M. Manmade Electromagnetic Fields and Oxidative Stress—Biological Effects and Consequences for Health. *Int. J. Mol. Sci.* **2021**, *22* (7), 3772.

(4) Pukkalla, S. K.; Subbarao, B. Evaluation of Critical Point-of-Entry (POE) Protection Devices for E1 & E2 Pulses as per MIL STD 188−125−1&2. In *2018 15th International Conference on Electromagnetic Interference & Compatibility (INCEMIC)*; IEEE: Bengaluru (Bangalore), India, 2018; pp 1−4. DOI: 10.1109/incemic.2018.8704567.

(5) Wanasinghe, D.; Aslani, F. A Review on Recent Advancement of Electromagnetic Interference Shielding Novel Metallic Materials and Processes. *Compos. Part B Eng.* **2019**, *176*, 107207.

(6) Tian, K.; Hu, D.; Wei, Q.; Fu, Q.; Deng, H. Recent Progress on Multifunctional Electromagnetic Interference Shielding Polymer Composites. *J. Mater. Sci. Technol.* **2023**, *134*, 106−131.

(7) Chen, Y.; Li, J.; Li, T.; Zhang, L.; Meng, F. Recent Advances in Graphene-Based Films for Electromagnetic Interference Shielding: Review and Future Prospects. *Carbon* **2021**, *180*, 163−184.

(8) Deng, B.; Liu, Z.; Peng, H. Toward Mass Production of CVD Graphene Films. *Adv. Mater.* **2019**, *31* (9), 1800996.

(9) Kausar, A.; Ahmad, I.; Zhao, T.; Aldaghri, O.; Ibnaouf, K. H.; Eisa, M. H.; Lam, T. D. Graphene Nanocomposites for Electromagnetic Interference Shielding—Trends and Advancements. *J. Compos. Sci.* **2023**, *7* (9), 384.

(10) Sun, J.; Zhou, D. Advances in Graphene-Polymer Nanocomposite Foams for Electromagnetic Interference Shielding. *Polymers* **2023**, *15* (15), 3235.

(11) Shahzad, F.; Kumar, P.; Yu, S.; Lee, S.; Kim, Y.-H.; Hong, S. M.; Koo, C. M. Sulfur-Doped Graphene Laminates for EMI Shielding Applications. *J. Mater. Chem. C* **2015**, *3* (38), 9802−9810.

(12) Li, X.; Qu, Y.; Wang, X.; Bian, H.; Wu, W.; Dai, H. Flexible Graphene/Silver Nanoparticles/Aluminum Film Paper for High-Performance Electromagnetic Interference Shielding. *Mater. Des.* **2022**, *213*, 110296.

(13) Liu, J.; Cui, L.; Losic, D. Graphene and Graphene Oxide as New Nanocarriers for Drug Delivery Applications. *Acta Biomater.* **2013**, *9* (12), 9243−9257.

(14) Han, T.-H.; Kim, H.; Kwon, S.-J.; Lee, T.-W. Graphene-Based Flexible Electronic Devices. *Mater. Sci. Eng. R Rep.* **2017**, *118*, 1−43.

(15) Qiao, Y.; Li, X.; Hirtz, T.; Deng, G.; Wei, Y.; Li, M.; Ji, S.; Wu, Q.; Jian, J.; Wu, F.; Shen, Y.; Tian, H.; Yang, Y.; Ren, T.-L. Graphene-Based Wearable Sensors. *Nanoscale* **2019**, *11* (41), 18923−18945.

(16) Ding, X.; Liu, H.; Fan, Y. Graphene-Based Materials in Regenerative Medicine. *Adv. Healthc. Mater.* **2015**, *4* (10), 1451−1468.

(17) Liu, D.; Gao, Y.; Song, Y.; Zhu, H.; Zhang, L.; Xie, Y.; Shi, H.; Shi, Z.; Yang, Q.; Xiong, C. Highly Sensitive Multifunctional Electronic Skin Based on Nanocellulose/MXene Composite Films with Good Electromagnetic Shielding Biocompatible Antibacterial Properties. *Biomacromolecules* **2022**, *23* (1), 182−195.

(18) Naghdi, S.; Jaleh, B.; Eslamipanah, M.; Moradi, A.; Abdollahi, M.; Einali, N.; Rhee, K. Y. Graphene Family, and Their Hybrid Structures for Electromagnetic Interference Shielding Applications: Recent Trends and Prospects. *J. Alloys Compd.* **2022**, *900*, 163176.

(19) Ramlow, H.; De Souza, G. B.; Fonseca, M. P.; Raizer, A.; Rambo, C. R.; Machado, R. A. F. Lightweight and Flexible Nanostructured C/SiCN Nanofiber Nonwoven for Electromagnetic Reflection Shielding of 5G C-Band Frequencies. *J. Mater. Sci. Mater. Electron.* **2023**, *34* (22), 1631.

(20) Shahzad, F.; Alhabeb, M.; Hatter, C. B.; Anasori, B.; Man Hong, S.; Koo, C. M.; Gogotsi, Y. Electromagnetic Interference Shielding with 2D Transition Metal Carbides (MXenes). *Science* **2016**, *353* (6304), 1137−1140.

(21) Sohi, N. J. S.; Rahaman, M.; Khastgir, D. Dielectric Property and Electromagnetic Interference Shielding Effectiveness of Ethylene Vinyl Acetate-based Conductive Composites: Effect of Different Type of Carbon Fillers. *Polym. Compos.* **2011**, *32* (7), 1148−1154.

(22) Radziuk, D.; Möhwald, H. Ultrasonically Treated Liquid Interfaces for Progress in Cleaning and Separation Processes. *Phys. Chem. Chem. Phys.* **2016**, *18* (1), 21−46.

(23) Xu, H.; Tang, T.; Man, Z.; Wu, X.; Zhao, H.; Liang, X.; Li, C. Research Status and Future Perspectives of Low Dimensional Electromagnetic Wave Absorption Materials. *J. Mater. Chem. C* **2023**, *11* (42), 14481−14494.

(24) Iqbal, A.; Sambyal, P.; Koo, C. M. 2D MXenes for Electromagnetic Shielding: A Review. *Adv. Funct. Mater.* **2020**, *30* (47), 2000883.

(25) Zhao, H.-B.; Fu, Z.-B.; Chen, H.-B.; Zhong, M.-L.; Wang, C.-Y. Excellent Electromagnetic Absorption Capability of Ni/Carbon Based Conductive and Magnetic Foams Synthesized via a Green One Pot Route. *ACS Appl. Mater. Interfaces* **2016**, *8* (2), 1468−1477.

(26) Kim, Y.; Hyeong, S.-K.; Choi, Y.; Lee, S.-K.; Lee, J.-H.; Yu, H. K. Transparent and Flexible Electromagnetic Interference Shielding Film Using ITO Nanobranches by Internal Scattering. *ACS Appl. Mater. Interfaces* **2021**, *13* (51), 61413−61421.

(27) Lee, S. H.; Yu, S.; Shahzad, F.; Kim, W. N.; Park, C.; Hong, S. M.; Koo, C. M. Density-Tunable Lightweight Polymer Composites with Dual-Functional Ability of Efficient EMI Shielding and Heat Dissipation. *Nanoscale* **2017**, *9* (36), 13432−13440.

(28) Hwang, C.; Cybart, S. A.; Shin, S. J.; Kim, S.; Kim, K.; Rappoport, T. G.; Wu, S. M.; Jozwiak, C.; Fedorov, A. V.; Mo, S.-K.; Lee, D.-H.; Min, B. I.; Haller, E. E.; Dynes, R. C.; Castro Neto, A. H.; Lanzara, A. Magnetic Effects in Sulfur-Decorated Graphene. *Sci. Rep.* **2016**, *6* (1), 21460.

(29) Tuček, J.; Błoński, P.; Sofer, Z.; Šimek, P.; Petr, M.; Pumera, M.; Otyepka, M.; Zbořil, R. Sulfur Doping Induces Strong Ferromagnetic Ordering in Graphene: Effect of Concentration and Substitution Mechanism. *Adv. Mater.* **2016**, *28* (25), 5045−5053.

(30) Tan, L.; Zhu, M.; Li, X.; Feng, H.; Chen, N.; Zhao, D. Lightweight Excellent Microwave Absorption Properties Based on Sulfur Doped Graphene. *J. Saudi Chem. Soc.* **2020**, *24* (1), 9−19.

(31) Quan, L.; Qin, F. X.; Lu, H. T.; Estevez, D.; Wang, Y. F.; Li, Y. H.; Tian, Y.; Wang, H.; Peng, H. X. Sequencing Dual Dopants for an Electromagnetic Tunable Graphene. *Chem. Eng. J.* **2021**, *413*, 127421.

(32) Zhao, H.; Cheng, Y.; Lv, H.; Ji, G.; Du, Y. A Novel Hierarchically Porous Magnetic Carbon Derived from Biomass for Strong Lightweight Microwave Absorption. *Carbon* **2019**, *142*, 245−253.

(33) Li, J.; Tsai, M.; Chiu, R.; He, E.; Hsieh, A.; Tsai, M.; Chu, F.; Chen, J. Y.; Jian, S.; Chen, S.; Wang, Y.-P. EMI Shielding Technology in 5G RF System in Package Module. In *2020 IEEE 70th Electronic Components and Technology Conference (ECTC)*; IEEE: Orlando, FL, USA, 2020; pp 931−937. DOI: 10.1109/ECTC32862.2020.00152.

(34) Lee, S.; Nguyen, N. K.; Kim, M.; Park, P.; Nah, J. Conductivity-Controlled Polyvinylidene Fluoride Nanofiber Stack for Absorption-Dominant Electromagnetic Interference Shielding Materials. *ACS Appl. Mater. Interfaces* **2023**, *15* (27), 33180−33189.

(35) Bahramian, R.; Nezafati, M. B.; Hamed Aboutalebi, S. Recent Progress and Prospects of Two-Dimensional Materials for Electromagnetic Interference Shielding. *FlatChem.* **2024**, *47*, 100722.

(36) Calheiros Souto, L. F.; Soares, B. G. Electromagnetic Wave Absorption, EMI Shielding Effectiveness and Electrical Properties of Ethylene - Vinyl Acetate (EVA)/ Polyaniline (PAni) Blends Prepared by in Situ Polymerization. *Synth. Met.* **2023**, *298*, 117441.

(37) Ding, Y.; Yang, Q.; Li, Y.; Yang, Z.; Wang, Z.; Liang, H.; Wu, S.-T. Waveguide-Based Augmented Reality Displays: Perspectives and Challenges. *eLight* **2023**, *3* (1), 24.

(38) Enconniere, J.; Ortiz-Carretero, J.; Pachidis, V. Mission Performance Analysis of a Conceptual Coaxial Rotorcraft for Air Taxi Applications. *Aerosp. Sci. Technol.* **2017**, *69*, 1−14.
(39) Seo, I. S.; Chin, W. S.; Lee, D. G. Characterization of Electromagnetic Properties of Polymeric Composite Materials with Free Space Method. *Compos. Struct.* **2004**, *66* (1−4), 533−542.
(40) Shen, B.; Zhai, W.; Zheng, W. Ultrathin Flexible Graphene Film: An Excellent Thermal Conducting Material with Efficient EMI Shielding. *Adv. Funct. Mater.* **2014**, *24* (28), 4542−4548.
(41) Jiang, X.; Zhao, Z.; Zhou, S.; Zou, H.; Liu, P. Anisotropic and Lightweight Carbon/Graphene Composite Aerogels for Efficient Thermal Insulation and Electromagnetic Interference Shielding. *ACS Appl. Mater. Interfaces* **2022**, *14* (40), 45844−45852.
(42) Feng, R.; Zhu, W.; Yang, W.; Li, S.; Zhang, C.; Li, Z.; Du, S.; Li, Y. Scalable Production of Flexible and Multifunctional Graphene-Based Polymer Composite Film for High-Performance Electromagnetic Interference Shielding. *Carbon* **2025**, *233*, 119875.
(43) Kumari, S.; Dalal, J.; Kumar, A.; Pal, R.; Chahal, R.; Ohlan, A. Enhanced Microwave Absorption Properties of Conducting Polymer@graphene Composite to Counteract Electromagnetic Radiation Pollution: Green EMI Shielding. *RSC Adv.* **2024**, *14* (1), 662−676.
(44) Zhi, Y.; Xu, J.; He, J.; Xu, J.; Zhang, H. Magnetic Field-Induced Aligned Graphene/Cellulose Conductive Composites for Electroluminescent Devices. *ACS Appl. Nano Mater.* **2023**, *6* (18), 17251−17262.
(45) Aboutalebi, S. H.; Gudarzi, M. M.; Zheng, Q. B.; Kim, J. Spontaneous Formation of Liquid Crystals in Ultralarge Graphene Oxide Dispersions. *Adv. Funct. Mater.* **2011**, *21* (15), 2978−2988.
(46) Austria, H. F. M.; T. M, S.; Setiawan, O.; Widakdo, J.; Chiao, Y.-H.; Hung, W.-S.; Wang, C.-F.; Hu, C.-C.; Lee, K.-R.; Lai, J.-Y. A Review on the Recent Advancements in Graphene-Based Membranes and Their Applications as Stimuli-Responsive Separation Materials. *J. Mater. Chem. A* **2021**, *9* (38), 21510−21531.
(47) Guo, S.; Chen, J.; Zhang, Y.; Liu, J. Graphene-Based Films: Fabrication, Interfacial Modification, and Applications. *Nanomaterials* **2021**, *11* (10), 2539.
(48) Wang, N.; Samani, M. K.; Li, H.; Dong, L.; Zhang, Z.; Su, P.; Chen, S.; Chen, J.; Huang, S.; Yuan, G.; Xu, X.; Li, B.; Leifer, K.; Ye, L.; Liu, J. Tailoring the Thermal and Mechanical Properties of Graphene Film by Structural Engineering. *Small* **2018**, *14* (29), 1801346.
(49) Sheath, P.; Majumder, M. Flux Accentuation and Improved Rejection in Graphene-Based Filtration Membranes Produced by Capillary-Force-Assisted Self-Assembly. *Philos. Trans. R. Soc. Math. Phys. Eng. Sci.* **2016**, *374* (2060), 20150028.
(50) Tkacz, R.; Oldenbourg, R.; Fulcher, A.; Miansari, M.; Majumder, M. Capillary-Force-Assisted Self-Assembly (CAS) of Highly Ordered and Anisotropic Graphene-Based Thin Films. *J. Phys. Chem. C* **2014**, *118* (1), 259−267.
(51) Wu, C.; Jiu, J.; Araki, T.; Koga, H.; Sekitani, T.; Wang, H.; Suganuma, K. Rapid Self-Assembly of Ultrathin Graphene Oxide Film and Application to Silver Nanowire Flexible Transparent Electrodes. *RSC Adv.* **2016**, *6* (19), 15838−15845.
(52) Liang, H.; Zang, X.; Liu, Y.; Chen, D.; Xu, Z.; Gao, W.; Wang, X.; Gao, C.; Chen, G.; Xue, M. Tailorable Graphene-Based Superconducting Films via Self-Assembly and in-Situ Doping. *Carbon* **2019**, *152*, 527−531.
(53) Wang, N.; Chen, S.; Nkansah, A.; Darmawan, C. C.; Ye, L.; Liu, J. Highly Thermally Conductive and Light Weight Copper/Graphene Film Laminated Composites for Cooling Applications. In *2018 19th International Conference on Electronic Packaging Technology (ICEPT)*; IEEE: Shanghai, 2018; pp 1588−1592. DOI: 10.1109/ICEPT.2018.8480614.
(54) Dieng, M.; Sankar, S.; Ni, P.; Florea, I.; Alpuim, P.; Capasso, A.; Yassar, A.; Bouanis, F. Z. Solution-Processed Functionalized Graphene Film Prepared by Vacuum Filtration for Flexible NO2 Sensors. *Sensors* **2023**, *23* (4), 1831.
(55) Dikin, D. A.; Stankovich, S.; Zimney, E. J.; Piner, R. D.; Dommett, G. H. B.; Evmenenko, G.; Nguyen, S. T.; Ruoff, R. S. Preparation and Characterization of Graphene Oxide Paper. *Nature* **2007**, *448* (7152), 457−460.
(56) Yang, W.; Zhao, Z.; Wu, K.; Huang, R.; Liu, T.; Jiang, H.; Chen, F.; Fu, Q. Ultrathin Flexible Reduced Graphene Oxide/Cellulose Nanofiber Composite Films with Strongly Anisotropic Thermal Conductivity and Efficient Electromagnetic Interference Shielding. *J. Mater. Chem. C* **2017**, *5* (15), 3748−3756.
(57) Chen, Y.; Hou, X.; Kang, R.; Liang, Y.; Guo, L.; Dai, W.; Nishimura, K.; Lin, C.-T.; Jiang, N.; Yu, J. Highly Flexible Biodegradable Cellulose Nanofiber/Graphene Heat-Spreader Films with Improved Mechanical Properties and Enhanced Thermal Conductivity. *J. Mater. Chem. C* **2018**, *6* (46), 12739−12745.
(58) Xiang, C.; Guo, R.; Lin, S.; Jiang, S.; Lan, J.; Wang, C.; Cui, C.; Xiao, H.; Zhang, Y. Lightweight and Ultrathin TiO2-Ti3C2TX/Graphene Film with Electromagnetic Interference Shielding. *Chem. Eng. J.* **2019**, *360*, 1158−1166.
(59) Zhang, X.; Guo, Y.; Liu, Y.; Li, Z.; Fang, W.; Peng, L.; Zhou, J.; Xu, Z.; Gao, C. Ultrathick and Highly Thermally Conductive Graphene Films by Self-Fusion. *Carbon* **2020**, *167*, 249−255.
(60) Ma, L.; Wang, Y.; Wang, Y.; Wang, C.; Gao, X. Graphene Induced Carbonization of Polyimide Films to Prepared Flexible Carbon Films with Improving-Thermal Conductivity. *Ceram. Int.* **2020**, *46* (3), 3332−3338.
(61) Lin, S.; Ju, S.; Zhang, J.; Shi, G.; He, Y.; Jiang, D. Ultrathin Flexible Graphene Films with High Thermal Conductivity and Excellent EMI Shielding Performance Using Large-Sized Graphene Oxide Flakes. *RSC Adv.* **2019**, *9* (3), 1419−1427.
(62) Chen, S.; Wang, Q.; Zhang, M.; Huang, R.; Huang, Y.; Tang, J.; Liu, J. Scalable Production of Thick Graphene Film for next Generation Thermal Management Application. *Carbon* **2020**, *167*, 270−277.
(63) Liu, Y.; Li, P.; Wang, F.; Fang, W.; Xu, Z.; Gao, W.; Gao, C. Rapid Roll-to-Roll Production of Graphene Films Using Intensive Joule Heating. *Carbon* **2019**, *155*, 462−468.
(64) Si, Y.; Jin, H.; Zhang, Q.; Xu, D.; Xu, R.; Ding, A.; Liu, D. Roll-to-Roll Processable MXene-rGO-PVA Composite Films with Enhanced Mechanical Properties and Environmental Stability for Electromagnetic Interference Shielding. *Ceram. Int.* **2022**, *48* (17), 24898−24905.
(65) Fang, X.; Fan, Z.; Gu, Y.; Shi, J.; Chen, M.; Chen, X.; Qiu, S.; Zabihi, F.; Eslamian, M.; Chen, Q. A Solution Processable Flexible Transparent Conductive Graphene/PEDOT: PSS Film Fabricated by Spin and Blade Coating. *J. Shanghai Jiaotong Univ. Sci.* **2018**, *23* (1), 106−111.
(66) Kim, S.-Y.; Gang, H.-E.; Park, G.-T.; Jeon, H.-B.; Jeong, Y. G. Microstructure and Electrothermal Characterization of Transparent Reduced Graphene Oxide Thin Films Manufactured by Spin-Coating and Thermal Reduction. *Results Phys.* **2021**, *24*, 104107.
(67) Ollik, K.; Lieder, M. Review of the Application of Graphene-Based Coatings as Anticorrosion Layers. *Coatings* **2020**, *10* (9), 883.
(68) Oytun, F.; Basarir, F. Spin-Assisted Layer-by-Layer Assembled Oppositely Charged Reduced Graphene Oxide Films. *Mater. Lett.* **2019**, *257*, 126756.
(69) Xiong, R.; Hu, K.; Grant, A. M.; Ma, R.; Xu, W.; Lu, C.; Zhang, X.; Tsukruk, V. V. Ultrarobust Transparent Cellulose Nanocrystal-Graphene Membranes with High Electrical Conductivity. *Adv. Mater.* **2016**, *28* (7), 1501−1509.
(70) Lee, T.; Min, S. H.; Gu, M.; Jung, Y. K.; Lee, W.; Lee, J. U.; Seong, D. G.; Kim, B.-S. Layer-by-Layer Assembly for Graphene-Based Multilayer Nanocomposites: Synthesis and Applications. *Chem. Mater.* **2015**, *27* (11), 3785−3796.
(71) Yadav, R. S.; Kuřitka, I.; Vilcakova, J.; Machovsky, M.; Skoda, D.; Urbánek, P.; Masař, M.; Jurča, M.; Urbánek, M.; Kalina, L.; Havlica, J. $NiFe_2O_4$ Nanoparticles Synthesized by Dextrin from Corn-Mediated Sol-Gel Combustion Method and Its Polypropylene Nanocomposites Engineered with Reduced Graphene Oxide for the Reduction of Electromagnetic Pollution. *ACS Omega* **2019**, *4* (26), 22069−22081.

(72) Kiran; Kumar, S.; Thakur, N. Structural, Dielectric, and Magnetic Properties of Reduced Graphene Oxide-Wrapped MnFe2O4 Composites Synthesized by in-Situ Sol-Gel Autocombustion Method. *Ceram. Int.* **2022**, *48* (4), 4444−4455.
(73) Chhetri, S.; Kuila, T. Polymer Composites with 3D Graphene Architectures as High-Performance EMI Shielding Materials: A Review. *RSC Appl. Polym.* **2024**, *2* (4), 507−533.
(74) Bobsin, A.; Menezes Kerber, R.; Fernandes, I. J.; Ferreira, S. B.; Hasenkamp, W.; Peter, C. R.; Michels-Brito, P. H.; Akanno, A.; Michels, L.; Raaen, S.; Fossum, J. O.; Moraes, C. A. M. Conductive Water-Based Graphene Suspension for Electromagnetic Interference Shielding via Spray Coating on SiP Module. *Prog. Org. Coat.* **2024**, *195*, 108658.
(75) Choi, J. R.; Han, J.; Yu, W.-R.; Lee, H. J.; Cho, S.; Jung, B. M.; Lee, S.-B. Facile Fabrication of Ultrathin Graphene/Cellulose Composites with Efficient Electromagnetic Interference Shielding by Spray Deposition. *Mater. Lett.* **2023**, *341*, 134264.
(76) Guan, R.; Zou, F.; Li, D.; Yao, Y. A High-Thermal-Stability, Fully Spray Coated Multilayer Thin-Film Graphene/Polyamide-Imide Nanocomposite Strain Sensor for Acquiring High-Frequency Ultrasonic Waves. *Compos. Sci. Technol.* **2022**, *227*, 109628.
(77) Ji, J.; Wang, Y.; Zhao, W.; Wang, G. Laser-Induced Graphene/TiCN on a Polyimide/MXene Film as Interference Shielding Materials for Terahertz Electromagnetic Waves. *ACS Appl. Nano Mater.* **2023**, *6* (24), 23401−23409.
(78) Huang, C.; Liang, M.; Wang, B.; Su, R.; Feng, Y.; Xing, W.; Zhao, X.; Bian, X.; You, Z.; You, R. In Situ Laser-Induced 3D Porous Graphene within Transparent Polymers for Encapsulation-Free and Tunable Ultrabroadband Terahertz Absorption. *ACS Appl. Mater. Interfaces* **2024**, *16* (20), 26557−26567.
(79) Yu, Z.; Yu, W.; Jiang, Y.; Wang, Z.; Zhao, W.; Liu, X. Upcycling of Polybenzoxazine to Magnetic Metal Nanoparticle-Doped Laser-Induced Graphene for Electromagnetic Interference Shielding. *ACS Appl. Nano Mater.* **2022**, *5* (9), 13158−13170.
(80) Ning, Y.; Zeng, X.; Huang, J.; Shen, Z.; Gao, Y.; Che, R. Multifunctional Electromagnetic Responsive Porous Materials Synthesized by Freeze Casting: Principles, Progress, and Prospects. *Adv. Funct. Mater.* **2025**, *35* (6), 2414838.
(81) Zhao, X.; Zhang, H.; Chan, K.-Y.; Huang, X.; Yang, Y.; Shen, X. Tree-Inspired Structurally Graded Aerogel with Synergistic Water, Salt, and Thermal Transport for High-Salinity Solar-Powered Evaporation. *Nano Micro Lett.* **2024**, *16* (1), 222.
(82) Dong, X.; Chan, K.-Y.; Yin, X.; Zhang, Y.; Zhao, X.; Yang, Y.; Wang, Z.; Shen, X. Anisotropic Hygroscopic Hydrogels with Synergistic Insulation-Radiation-Evaporation for High-Power and Self-Sustained Passive Daytime Cooling. *Nano Micro Lett.* **2025**, *17* (1), 240.
(83) Chan, K.-Y.; Dong, X.; Yang, Y.; Zhao, X.; Li, D.; Xu, M.; Yin, X.; Wang, Z.; Shen, X. A Heterogeneous Nanocomposite Architecture with Contrasting Thermal Conductivity and Hydrophilicity for Synergistic Solar-Thermal Storage and Evaporation. *Mater. Horiz.* **2025**, *12* (14), 5175−5186.
(84) Chan, K.-Y.; Shen, X.; Yang, J.; Lin, K.-T.; Venkatesan, H.; Kim, E.; Zhang, H.; Lee, J.-H.; Yu, J.; Yang, J.; Kim, J.-K. Scalable Anisotropic Cooling Aerogels by Additive Freeze-Casting. *Nat. Commun.* **2022**, *13* (1), 5553.
(85) Chang, J.; Zhai, H.; Hu, Z.; Li, J. Ultra-Thin Metal Composites for Electromagnetic Interference Shielding. *Compos. Part B Eng.* **2022**, *246*, 110269.
(86) Zhang, Y.; Dong, H.; Li, Q.; Mou, N.; Chen, L.; Zhang, L. Double-Layer Metal Mesh Etched by Femtosecond Laser for High-Performance Electromagnetic Interference Shielding Window. *RSC Adv.* **2019**, *9* (39), 22282−22287.
(87) Shi, K.; Su, J.; Hu, K.; Liang, H. High-Performance Copper Mesh for Optically Transparent Electromagnetic Interference Shielding. *J. Mater. Sci. Mater. Electron.* **2020**, *31* (14), 11646−11653.
(88) Ayub, S.; Guan, B. H.; Ahmad, F.; Javed, M. F.; Mosavi, A.; Felde, I. Preparation Methods for Graphene Metal and Polymer Based Composites for EMI Shielding Materials: State of the Art Review of the Conventional and Machine Learning Methods. *Metals* **2021**, *11* (8), 1164.
(89) Omastová, M.; Kosina, S.; Pionteck, J.; Janke, A.; Pavlinec, J. Electrical Properties and Stability of Polypyrrole Containing Conducting Polymer Composites. *Synth. Met.* **1996**, *81* (1), 49−57.
(90) Omastová, M.; Trchová, M.; Pionteck, J.; Prokeš, J.; Stejskal, J. Effect of Polymerization Conditions on the Properties of Polypyrrole Prepared in the Presence of Sodium Bis(2-Ethylhexyl) Sulfosuccinate. *Synth. Met.* **2004**, *143* (2), 153−161.
(91) Yu, D.; Wang, Y.; Hao, T.; Wang, W.; Liu, B. Preparation of Silver-Plated Polyimide Fabric Initiated by Polyaniline with Electromagnetic Shielding Properties. *J. Ind. Text.* **2018**, *47* (6), 1392−1406.
(92) Jagatheesan, K.; Ramasamy, A.; Das, A.; Basu, A. Electromagnetic Shielding Behaviour of Conductive Filler Composites and Conductive Fabrics - a Review. *Indian J. Fibre Text Res.* **2014**, *39* (3), 329−342.
(93) Pawar, S. P.; Rzeczkowski, P.; Pötschke, P.; Krause, B.; Bose, S. Does the Processing Method Resulting in Different States of an Interconnected Network of Multiwalled Carbon Nanotubes in Polymeric Blend Nanocomposites Affect EMI Shielding Properties? *ACS Omega* **2018**, *3* (5), 5771−5782.
(94) Wang, Y.; Cheng, X.-D.; Song, W.-L.; Ma, C.-J.; Bian, X.-M.; Chen, M. Hydro-Sensitive Sandwich Structures for Self-Tunable Smart Electromagnetic Shielding. *Chem. Eng. J.* **2018**, *344*, 342−352.
(95) Bhattacharjee, Y.; Bhingardive, V.; Biswas, S.; Bose, S. Construction of a Carbon Fiber Based Layer-by-Layer (LbL) Assembly - a Smart Approach towards Effective EMI Shielding. *RSC Adv.* **2016**, *6* (113), 112614−112619.
(96) Wang, Z.; Wei, R.; Liu, X. Fluffy and Ordered Graphene Multilayer Films with Improved Electromagnetic Interference Shielding over X-Band. *ACS Appl. Mater. Interfaces* **2017**, *9* (27), 22408−22419.
(97) Yuan, J.-K.; Yao, S.-H.; Sylvestre, A.; Bai, J. Biphasic Polymer Blends Containing Carbon Nanotubes: Heterogeneous Nanotube Distribution and Its Influence on the Dielectric Properties. *J. Phys. Chem. C* **2012**, *116* (2), 2051−2058.
(98) Eswaraiah, V.; Sankaranarayanan, V.; Ramaprabhu, S. Functionalized Graphene-PVDF Foam Composites for EMI Shielding. *Macromol. Mater. Eng.* **2011**, *296* (10), 894−898.
(99) Ushak, S.; Gutierrez, A.; Galleguillos, H.; Fernandez, A. G.; Cabeza, L. F.; Grágeda, M. Thermophysical Characterization of a By-Product from the Non-Metallic Industry as Inorganic PCM. *Sol. Energy Mater. Sol. Cells* **2015**, *132*, 385−391.
(100) Ossi, P. M.; Pastorelli, R. Structural Stability of Irradiated Metallic and Non-Metallic Films. *Surf. Coat. Technol.* **2000**, *125* (1−3), 61−65.
(101) Lopes, C. M. A.; Peixoto, G. G.; Rezende, M. C. Microwave Absorption Effectiveness of Nonwoven Support Impregnated with Carbon Black. In *Proceedings of the 2003 SBMO/IEEE MTT-S International Microwave and Optoelectronics Conference - IMOC 2003. (Cat. No.03TH8678)*; IEEE: Foz do Iguacu, Brazil, 2003; Vol. 2, pp 771−774. DOI: 10.1109/IMOC.2003.1242676.
(102) Zhu, H.; Chen, P.; Wu, R.; Zhang, H. Microwave Absorption Properties of Carbon Fibre Containing Nonwovens. *Indian J. Fibre Text Res.* **2007**, *32* (4), 391.
(103) Wu, J.; Chung, D. D. L. Increasing the Electromagnetic Interference Shielding Effectiveness of Carbon Fiber Polymer-Matrix Composite by Using Activated Carbon Fibers. *Carbon* **2002**, *40* (3), 445−447.
(104) Nahil, M. A.; Williams, P. T. Recycling of Carbon Fibre Reinforced Polymeric Waste for the Production of Activated Carbon Fibres. *J. Anal. Appl. Pyrolysis* **2011**, *91* (1), 67−75.
(105) Zhou, Y.; Gaur, A.; Hur, S.-H.; Kocabas, C.; Meitl, M. A.; Shim, M.; Rogers, J. A. P-Channel, n-Channel Thin Film Transistors and P-n Diodes Based on Single Wall Carbon Nanotube Networks. *Nano Lett.* **2004**, *4* (10), 2031−2035.
(106) Takenobu, T.; Takano, T.; Shiraishi, M.; Murakami, Y.; Ata, M.; Kataura, H.; Achiba, Y.; Iwasa, Y. Stable and Controlled

Amphoteric Doping by Encapsulation of Organic Molecules inside Carbon Nanotubes. *Nat. Mater.* **2003**, *2* (10), 683−688.
(107) Vázquez, E.; Prato, M. Carbon Nanotubes and Microwaves: Interactions, Responses, and Applications. *ACS Nano* **2009**, *3* (12), 3819−3824.
(108) Liu, Z.; Bai, G.; Huang, Y.; Li, F.; Ma, Y.; Guo, T.; He, X.; Lin, X.; Gao, H.; Chen, Y. Microwave Absorption of Single-Walled Carbon Nanotubes/Soluble Cross-Linked Polyurethane Composites. *J. Phys. Chem. C* **2007**, *111* (37), 13696−13700.
(109) Saib, A.; Bednarz, L.; Daussin, R.; Bailly, C.; Lou, X.; Thomassin, J.-M.; Pagnoulle, C.; Detrembleur, C.; Jerome, R.; Huynen, I. Carbon Nanotube Composites for Broadband Microwave Absorbing Materials. *IEEE Trans. Microw. Theory Technol.* **2006**, *54* (6), 2745−2754.
(110) Yue, L.; Guo, H.; Wang, X.; Sun, T.; Liu, H.; Li, Q.; Xu, M.; Yang, Y.; Yang, W. Non-Metallic Element Modified Metal-Organic Frameworks as High-Performance Electrodes for All-Solid-State Asymmetric Supercapacitors. *J. Colloid Interface Sci.* **2019**, *539*, 370−378.
(111) Shen, Y.; Zhu, Z.; Xu, Z.; Li, Y. Recent Progress in 2D Inorganic Non-Conductive Materials for Alkali Metal-Based Batteries. *Energy Adv.* **2024**, *3* (8), 1844−1868.
(112) Fazli, A.; Moosaei, R.; Sharif, M.; Jamali Ashtiani, S. Developments of Graphene-Based Polymer Composites Processing Based on Novel Methods for Innovative Applications in Newborn Technologies. *Indian J. Sci. Technol.* **2015**, *8* (S9), 38.
(113) Carotenuto, G.; Romeo, V.; Cannavaro, I.; Roncato, D.; Martorana, B.; Gosso, M. Graphene-Polymer Composites. *IOP Conf. Ser. Mater. Sci. Eng.* **2012**, *40*, 012018.
(114) Li, X.; Magnuson, C. W.; Venugopal, A.; An, J.; Suk, J. W.; Han, B.; Borysiak, M.; Cai, W.; Velamakanni, A.; Zhu, Y.; Fu, L.; Vogel, E. M.; Voelkl, E.; Colombo, L.; Ruoff, R. S. Graphene Films with Large Domain Size by a Two-Step Chemical Vapor Deposition Process. *Nano Lett.* **2010**, *10* (11), 4328−4334.
(115) Xu, X.; Zhang, Z.; Dong, J.; Yi, D.; Niu, J.; Wu, M.; Lin, L.; Yin, R.; Li, M.; Zhou, J.; Wang, S.; Sun, J.; Duan, X.; Gao, P.; Jiang, Y.; Wu, X.; Peng, H.; Ruoff, R. S.; Liu, Z.; Yu, D.; Wang, E.; Ding, F.; Liu, K. Ultrafast Epitaxial Growth of Metre-Sized Single-Crystal Graphene on Industrial Cu Foil. *Sci. Bull.* **2017**, *62* (15), 1074−1080.
(116) Yoon, T.; Shin, W. C.; Kim, T. Y.; Mun, J. H.; Kim, T.-S.; Cho, B. J. Direct Measurement of Adhesion Energy of Monolayer Graphene As-Grown on Copper and Its Application to Renewable Transfer Process. *Nano Lett.* **2012**, *12* (3), 1448−1452.
(117) Dean, C. R.; Young, A. F.; Meric, I.; Lee, C.; Wang, L.; Sorgenfrei, S.; Watanabe, K.; Taniguchi, T.; Kim, P.; Shepard, K. L.; Hone, J. Boron Nitride Substrates for High-Quality Graphene Electronics. *Nat. Nanotechnol.* **2010**, *5* (10), 722−726.
(118) Chandrasekaran, S.; Sato, N.; Tölle, F.; Mülhaupt, R.; Fiedler, B.; Schulte, K. Fracture Toughness and Failure Mechanism of Graphene Based Epoxy Composites. *Compos. Sci. Technol.* **2014**, *97*, 90−99.
(119) Panahi-Sarmad, M.; Noroozi, M.; Xiao, X.; Park, C. B. Recent Advances in Graphene-Based Polymer Nanocomposites and Foams for Electromagnetic Interference Shielding Applications. *Ind. Eng. Chem. Res.* **2022**, *61* (4), 1545−1568.
(120) Bortz, D. R.; Heras, E. G.; Martin-Gullon, I. Impressive Fatigue Life and Fracture Toughness Improvements in Graphene Oxide/Epoxy Composites. *Macromolecules* **2012**, *45* (1), 238−245.
(121) Yao, L.; Cao, W.; Zhao, J.; Zheng, Q.; Wang, Y.; Jiang, S.; Pan, Q.; Song, J.; Zhu, Y.; Cao, M. Regulating Bifunctional Flower-like NiFe2O4/Graphene for Green EMI Shielding and Lithium Ion Storage. *J. Mater. Sci. Technol.* **2022**, *127*, 48−60.
(122) Yan, R.; Huang, Z.; Chen, Y.; Zhang, L.; Sheng, X. Phase Change Composite Based on Lignin Carbon Aerogel/Nickel Foam Dual-Network for Multisource Energy Harvesting and Superb EMI Shielding. *Int. J. Biol. Macromol.* **2024**, *277*, 134233.
(123) Wang, Y.; Yao, L.; Zheng, Q.; Cao, M.-S. Graphene-Wrapped Multiloculated Nickel Ferrite: A Highly Efficient Electromagnetic Attenuation Material for Microwave Absorbing and Green Shielding. *Nano Res.* **2022**, *15* (7), 6751−6760.
(124) Liang, L.; Xu, P.; Wang, Y.; Shang, Y.; Ma, J.; Su, F.; Feng, Y.; He, C.; Wang, Y.; Liu, C. Flexible Polyvinylidene Fluoride Film with Alternating Oriented Graphene/Ni Nanochains for Electromagnetic Interference Shielding and Thermal Management. *Chem. Eng. J.* **2020**, *395*, 125209.
(125) Dalal, J.; Malik, S.; Dahiya, S.; Punia, R.; Singh, K.; Maan, A. S.; Dhawan, S. K.; Ohlan, A. One Pot Synthesis and Electromagnetic Interference Shielding Behavior of Reduced Graphene Oxide Nanocomposites Decorated with Ni0.5Co0.5Fe2O4 Nanoparticles. *J. Alloys Compd.* **2021**, *887*, 161472.
(126) Zhan, Y.; Wang, J.; Zhang, K.; Li, Y.; Meng, Y.; Yan, N.; Wei, W.; Peng, F.; Xia, H. Fabrication of a Flexible Electromagnetic Interference Shielding Fe3O4@reduced Graphene Oxide/Natural Rubber Composite with Segregated Network. *Chem. Eng. J.* **2018**, *344*, 184−193.
(127) Guo, Y.; Qiu, H.; Ruan, K.; Zhang, Y.; Gu, J. Hierarchically Multifunctional Polyimide Composite Films with Strongly Enhanced Thermal Conductivity. *Nano-Micro Lett.* **2022**, *14* (1), 26.
(128) Chen, Y.; Wang, Y.; Zhang, H.-B.; Li, X.; Gui, C.-X.; Yu, Z.-Z. Enhanced Electromagnetic Interference Shielding Efficiency of Polystyrene/Graphene Composites with Magnetic Fe3O4 Nanoparticles. *Carbon* **2015**, *82*, 67−76.
(129) Liu, X.; Chen, T.; Liang, H.; Qin, F.; Yang, H.; Guo, X. Facile Approach for a Robust Graphene/Silver Nanowires Aerogel with High-Performance Electromagnetic Interference Shielding. *RSC Adv.* **2019**, *9* (1), 27−33.
(130) Zhang, N.; Wang, Z.; Song, R.; Wang, Q.; Chen, H.; Zhang, B.; Lv, H.; Wu, Z.; He, D. Flexible and Transparent Graphene/Silver-Nanowires Composite Film for High Electromagnetic Interference Shielding Effectiveness. *Sci. Bull.* **2019**, *64* (8), 540−546.
(131) Li, L.; Wang, M.; Guo, J.; Cao, M.; Qiu, H.; Yang, Z. Electrochemically Synthesized Ag/Graphene for Electromagnetic-Interference Shielding. *Mater. Res. Express* **2018**, *5* (12), 125604.
(132) Nasrollahzadeh, M.; Babaei, F.; Fakhri, P.; Jaleh, B. Synthesis, Characterization, Structural, Optical Properties and Catalytic Activity of Reduced Graphene Oxide/Copper Nanocomposites. *RSC Adv.* **2015**, *5* (14), 10782−10789.
(133) Naghdi, S.; Sajjadi, M.; Nasrollahzadeh, M.; Rhee, K. Y.; Sajadi, S. M.; Jaleh, B. Cuscuta Reflexa Leaf Extract Mediated Green Synthesis of the Cu Nanoparticles on Graphene Oxide/Manganese Dioxide Nanocomposite and Its Catalytic Activity toward Reduction of Nitroarenes and Organic Dyes. *J. Taiwan Inst. Chem. Eng.* **2018**, *86*, 158−173.
(134) Fakhri, P.; Jaleh, B.; Nasrollahzadeh, M. Synthesis and Characterization of Copper Nanoparticles Supported on Reduced Graphene Oxide as a Highly Active and Recyclable Catalyst for the Synthesis of Formamides and Primary Amines. *J. Mol. Catal. Chem.* **2014**, *383*−*384*, 17−22.
(135) Xu, Z.; Liang, M.; He, X.; Long, Q.; Yu, J.; Xie, K.; Liao, L. The Preparation of Carbonized Silk Cocoon-Co-Graphene Composite and Its Enhanced Electromagnetic Interference Shielding Performance. *Compos. Part Appl. Sci. Manuf.* **2019**, *119*, 111−118.
(136) Wang, X.; Jiang, H. T.; Yang, K. Y.; Ju, A. X.; Ma, C. Q.; Yu, X. L. Carbon Fiber Enhanced Mechanical and Electromagnetic Absorption Properties of Magnetic Graphene-Based Film. *Thin Solid Films* **2019**, *674*, 97−102.
(137) Drakakis, E.; Suchea, M.; Tudose, V.; Kenanakis, G.; Stratakis, D.; Dangakis, K.; Miaoudakis, A.; Vernardou, D.; Koudoumas, E. Zinc Oxide-Graphene Based Composite Layers for Electromagnetic Interference Shielding in the GHz Frequency Range. *Thin Solid Films* **2018**, *651*, 152−157.
(138) Naghdi, S.; Rhee, K. Y.; Hui, D.; Park, S. J. A Review of Conductive Metal Nanomaterials as Conductive, Transparent, and Flexible Coatings, Thin Films, and Conductive Fillers: Different Deposition Methods and Applications. *Coatings* **2018**, *8* (8), 278.
(139) Khodiri, A. A.; Al-Ashry, M. Y.; El-Shamy, A. G. Novel Hybrid Nanocomposites Based on Polyvinyl Alcohol/Graphene/Magnetite

https://doi.org/10.1021/acsaenm.5c00207
ACS Appl. Eng. Mater. 2025, 3, 2234−2258

Nanoparticles for High Electromagnetic Shielding Performance. *J. Alloys Compd.* **2020**, *847*, 156430.
(140) Lai, D.; Chen, X.; Liu, X.; Wang, Y. Flexible Poly(Vinyl Alcohol)/Reduced Graphene Oxide Coated Carbon Composites for Electromagnetic Interference Shielding. *ACS Appl. Nano Mater.* **2018**, *1* (10), 5854−5864.
(141) Li, T.-T.; Yan, M.; Jiang, Q.; Peng, H.-K.; Lin, J.-H.; Lou, C.-W. Characterization and Microstructure of Linear Electrode-Electrospun Graphene-Filled Polyvinyl Alcohol Nanofiber Films. *Materials* **2018**, *11* (6), 1033.
(142) Marka, S. K.; Sindam, B.; James Raju, K. C.; Srikanth, V. V. S. S. Flexible Few-Layered Graphene/Poly Vinyl Alcohol Composite Sheets: Synthesis, Characterization and EMI Shielding in X-Band through the Absorption Mechanism. *RSC Adv.* **2015**, *5* (46), 36498−36506.
(143) Rani, P.; Ahamed, B.; Deshmukh, K. Electromagnetic Interference Shielding Properties of Graphene Quantum-Dots Reinforced Poly(Vinyl Alcohol)/Polypyrrole Blend Nanocomposites. *J. Appl. Polym. Sci.* **2020**, *137* (45), 49392.
(144) Araújo, M. K. S.; Carvalho, A. S.; Santos, A. R.; Padrón-Hernández, E.; Falcão, E. H. L. Influence of Graphene Oxide and Reduced Graphene Oxide on TiO2-Reinforced Flexible Poly(Vinyl Alcohol) Films for Electromagnetic Interference Shielding. *J. Alloys Compd.* **2025**, *1010*, 177671.
(145) Li, J.; Li, J.; Li, T.; Xu, Z.; Chen, Y.; Zhang, L.; Qi, Q.; Liang, B.; Meng, F. Flexible and Excellent Electromagnetic Interference Shielding Film with Porous Alternating PVA-Derived Carbon and Graphene Layers. *iScience* **2023**, *26* (10), 107975.
(146) Bagotia, N.; Mohite, H.; Tanaliya, N.; Sharma, D. K. A Comparative Study of Electrical, EMI Shielding and Thermal Properties of Graphene and Multiwalled Carbon Nanotube Filled Polystyrene Nanocomposites. *Polym. Compos.* **2018**, DOI: 10.1002/pc.24465.
(147) Bera, R.; Suin, S.; Maiti, S.; Shrivastava, N. K.; Khatua, B. B. Carbon Nanohorn and Graphene Nanoplate Based Polystyrene Nanocomposites for Superior Electromagnetic Interference Shielding Applications. *J. Appl. Polym. Sci.* **2015**, *132* (46), app.42803.
(148) Das, M.; Sethy, P. P.; Sundaray, B. EMI Shielding Performance of Graphene Oxide Reinforced Polyaniline/Polystyrene Solution Cast Thin Films. *Synth. Met.* **2023**, *296*, 117369.
(149) Ghosh, S. K.; Paul, S.; Ghosh, T.; Das, N. Ch. Design of Interconnected Graphene Loaded Thermoplastic Elastomeric Blend Composite Films for Minimizing Electromagnetic Radiation and Efficient Heat Management. *Polym. Adv. Technol.* **2024**, *35* (7), No. e6510.
(150) Karteri, I.; Altun, M.; Gunes, M. Electromagnetic Interference Shielding Performance and Electromagnetic Properties of Wood-Plastic Nanocomposite with Graphene Nanoplatelets. *J. Mater. Sci. Mater. Electron.* **2017**, *28* (9), 6704−6711.
(151) Yao, K.; Gong, J.; Tian, N.; Lin, Y.; Wen, X.; Jiang, Z.; Na, H.; Tang, T. Flammability Properties and Electromagnetic Interference Shielding of PVC/Graphene Composites Containing Fe_3O_4 Nanoparticles. *RSC Adv.* **2015**, *5* (40), 31910−31919.
(152) Shahzad, M.; Shahid, S.; Rehan, Z. A.; Zhao, T.; Fatima, K.; Shakir, Hm. F.; Shahid, I. Enhanced Electromagnetic Interference Shielding Using Nanosilver-Decorated Graphene/Poly(Vinyl Chloride) Nanocomposite Films. *Mater. Chem. Phys.* **2024**, *314*, 128817.
(153) Cataldi, P.; Papageorgiou, D. G.; Pinter, G.; Kretinin, A. V.; Sampson, W. W.; Young, R. J.; Bissett, M.; Kinloch, I. A. Graphene-Polyurethane Coatings for Deformable Conductors and Electromagnetic Interference Shielding. *Adv. Electron. Mater.* **2020**, *6* (9), 2000429.
(154) Jiang, Q.; Liao, X.; Li, J.; Chen, J.; Wang, G.; Yi, J.; Yang, Q.; Li, G. Flexible Thermoplastic Polyurethane/Reduced Graphene Oxide Composite Foams for Electromagnetic Interference Shielding with High Absorption Characteristic. *Compos. Part Appl. Sci. Manuf.* **2019**, *123*, 310−319.
(155) Barani, Z.; Kargar, F.; Mohammadzadeh, A.; Naghibi, S.; Lo, C.; Rivera, B.; Balandin, A. A. Multifunctional Graphene Composites for Electromagnetic Shielding and Thermal Management at Elevated Temperatures. *Adv. Electron. Mater.* **2020**, *6* (11), 2000520.
(156) Qing, Y.; Li, Y.; Luo, F. Electromagnetic Interference Shielding Properties of Nitrogen-Doped Graphene/Epoxy Composites. *J. Mater. Sci. Mater. Electron.* **2021**, *32* (21), 25649−25655.
(157) Wang, S.; Xu, Y.; Ma, Y.; Sun, X.; Gong, Y.; Li, Y. Multifunctional Nanocomposites Reinforced by Aligned Graphene Network via a Low-Cost Lyophilization-Free Method. *Compos. Sci. Technol.* **2023**, *243*, 110250.
(158) Kanwal, R.; Maqsood, M. F.; Raza, M. A.; Inam, A.; Waris, M.; Rehman, Z. U.; Mehdi, S. M. Z.; Abbas, N.; Lee, N. Polypyrrole Coated Carbon Fiber/ Magnetite/ Graphene Oxide Reinforced Hybrid Epoxy Composites for High Strength and Electromagnetic Interference Shielding. *Mater. Today Commun.* **2024**, *38*, 107684.
(159) Salari, M.; Sansone, N. D.; Razzaz, Z.; Taromsari, S. M.; Leroux, M.; Park, C. B.; Lee, P. C. Insights into Synergy-Induced Multifunctional Property Enhancement Mechanisms in Hybrid Graphene Nanoplatelet Reinforced Polymer Composites. *Chem. Eng. J.* **2023**, *463*, 142406.
(160) Zhou, J.; Liu, C.; Xia, L.; Wang, L.; Qi, C.; Zhang, G.; Tan, Z.; Ren, B.; Yuan, B. Bridge-Graphene Connecting Polymer Composite with a Distinctive Segregated Structure for Simultaneously Improving Electromagnetic Interference Shielding and Flame-Retardant Properties. *Colloids Surf. Physicochem. Eng. Asp.* **2023**, *661*, 130853.
(161) Cai, J.; Ruffieux, P.; Jaafar, R.; Bieri, M.; Braun, T.; Blankenburg, S.; Muoth, M.; Seitsonen, A. P.; Saleh, M.; Feng, X.; Müllen, K.; Fasel, R. Atomically Precise Bottom-up Fabrication of Graphene Nanoribbons. *Nature* **2010**, *466* (7305), 470−473.
(162) Buzaglo, M.; Ruse, E.; Levy, I.; Nadiv, R.; Reuveni, G.; Shtein, M.; Regev, O. Top-down, Scalable Graphene Sheets Production: It Is All about the Precipitate. *Chem. Mater.* **2017**, *29* (23), 9998−10006.
(163) Tour, J. M. Top-down versus Bottom-up Fabrication of Graphene-Based Electronics. *Chem. Mater.* **2014**, *26* (1), 163−171.
(164) Zhang, Z.; Fraser, A.; Ye, S.; Merle, G.; Barralet, J. Top-down Bottom-up Graphene Synthesis. *Nano Futur.* **2019**, *3* (4), 42003.
(165) Novoselov, K. S.; Geim, A. K.; Morozov, S. V.; Jiang, D.; Zhang, Y.; Dubonos, S. V.; Grigorieva, I. V.; Firsov, A. A. Electric Field Effect in Atomically Thin Carbon Films. *Science* **2004**, *306* (5696), 666−669.
(166) Li, X.; Cai, W.; An, J.; Kim, S.; Nah, J.; Yang, D.; Piner, R.; Velamakanni, A.; Jung, I.; Tutuc, E.; Banerjee, S. K.; Colombo, L.; Ruoff, R. S. Large-Area Synthesis of High-Quality and Uniform Graphene Films on Copper Foils. *Science* **2009**, *324* (5932), 1312−1314.
(167) Hu, X.; Chen, L.; Zhang, Y.; Hu, Q.; Yang, J.; Chen, Y. Large-Scale Flexible and Highly Conductive Carbon Transparent Electrodes via Roll-to-Roll Process and Its High Performance Lab-Scale Indium Tin Oxide-Free Polymer Solar Cells. *Chem. Mater.* **2014**, *26* (21), 6293−6302.
(168) Hwang, U.; Kim, J.; Seol, M.; Lee, B.; Park, I.-K.; Suhr, J.; Nam, J.-D. Quantitative Interpretation of Electromagnetic Interference Shielding Efficiency: Is It Really a Wave Absorber or a Reflector? *ACS Omega* **2022**, *7* (5), 4135−4139.
(169) Song, W.-L.; Cao, M.-S.; Lu, M.-M.; Bi, S.; Wang, C.-Y.; Liu, J.; Yuan, J.; Fan, L.-Z. Flexible Graphene/Polymer Composite Films in Sandwich Structures for Effective Electromagnetic Interference Shielding. *CARBON* **2014**, *66*, 67−76.
(170) Gupta, T. K.; Singh, B. P.; Mathur, R. B.; Dhakate, S. R. Multi-Walled Carbon Nanotube-Graphene-Polyaniline Multiphase Nanocomposite with Superior Electromagnetic Shielding Effectiveness. *NANOSCALE* **2014**, *6* (2), 842−851.
(171) Wen, B.; Cao, M.; Lu, M.; Cao, W.; Shi, H.; Liu, J.; Wang, X.; Jin, H.; Fang, X.; Wang, W.; Yuan, J. Reduced Graphene Oxides: Light-Weight and High-Efficiency Electromagnetic Interference Shielding at Elevated Temperatures. *Adv. Mater.* **2014**, *26* (21), 3484−3489.
(172) Kumar, P.; Shahzad, F.; Yu, S.; Hong, S. M.; Kim, Y.-H.; Koo, C. M. Large-Area Reduced Graphene Oxide Thin Film with Excellent

Thermal Conductivity and Electromagnetic Interference Shielding Effectiveness. *CARBON* **2015**, *94*, 494−500.
(173) Zeng, Z.; Jin, H.; Chen, M.; Li, W.; Zhou, L.; Zhang, Z. Lightweight and Anisotropic Porous MWeNT/WPU Composites for Ultrahigh Performance Electromagnetic Interference Shielding. *Adv. Funct. Mater.* **2016**, *26* (2), 303−310.
(174) Shen, B.; Li, Y.; Yi, D.; Zhai, W.; Wei, X.; Zheng, W. Microcellular Graphene Foam for Improved Broadband Electromagnetic Interference Shielding. *CARBON* **2016**, *102*, 154−160.
(175) Sun, R.; Zhang, H.-B.; Liu, J.; Xie, X.; Yang, R.; Li, Y.; Hong, S.; Yu, Z.-Z. Highly Conductive Transition Metal Carbide/Carbonitride(MXene)@polystyrene Nanocomposites Fabricated by Electrostatic Assembly for Highly Efficient Electromagnetic Interference Shielding. *Adv. Funct. Mater.* **2017**, DOI: 10.1002/adfm.201702807.
(176) Liu, J.; Zhang, H.-B.; Sun, R.; Liu, Y.; Liu, Z.; Zhou, A.; Yu, Z.-Z. Hydrophobic, Flexible, and Lightweight MXene Foams for High-Performance Electromagnetic-Interference Shielding. *Adv. Mater.* **2017**, DOI: 10.1002/adma.201702367.
(177) Wu, Y.; Wang, Z.; Liu, X.; Shen, X.; Zheng, Q.; Xue, Q.; Kim, J.-K. Ultralight Graphene Foam/Conductive Polymer Composites for Exceptional Electromagnetic Interference Shielding. *ACS Appl. Mater. INTERFACES* **2017**, *9* (10), 9059−9069.
(178) Song, Q.; Ye, F.; Yin, X.; Li, W.; Li, H.; Liu, Y.; Li, K.; Xie, K.; Li, X.; Fu, Q.; Cheng, L.; Zhang, L.; Wei, B. Carbon Nanotube-Multilayered Graphene Edge Plane Core-Shell Hybrid Foams for Ultrahigh-Performance Electromagnetic-Interference Shielding. *Adv. Mater.* **2017**, DOI: 10.1002/adma.201701583.
(179) Cao, W.-T.; Chen, F.-F.; Zhu, Y.-J.; Zhang, Y.-G.; Jiang, Y.-Y.; Ma, M.-G.; Chen, F. Binary Strengthening and Toughening of MXene/Cellulose Nanofiber Composite Paper with Nacre-Inspired Structure and Superior Electromagnetic Interference Shielding Properties. *ACS Nano* **2018**, *12* (5), 4583−4593.
(180) Weng, G.-M.; Li, J.; Alhabeb, M.; Karpovich, C.; Wang, H.; Lipton, J.; Maleski, K.; Kong, J.; Shaulsky, E.; Elimelech, M.; Gogotsi, Y.; Taylor, A. D. Layer-by-Layer Assembly of Cross-Functional Semi-Transparent MXene-Carbon Nanotubes Composite Films for Next-Generation Electromagnetic Interference Shielding. *Adv. Funct. Mater.* **2018**, DOI: 10.1002/adfm.201803360.
(181) Cao, W.; Ma, C.; Tan, S.; Ma, M.; Wan, P.; Chen, F. Ultrathin and Flexible CNTs/MXene/Cellulose Nanofibrils Composite Paper for Electromagnetic Interference Shielding. *Nano-Micro Lett.* **2019**, DOI: 10.1007/s40820-019-0304-y.
(182) Iqbal, A.; Shahzad, F.; Hantanasirisakul, K.; Kim, M.-K.; Kwon, J.; Hong, J.; Kim, H.; Kim, D.; Gogotsi, Y.; Koo, C. M. Anomalous Absorption of Electromagnetic Waves by 2D Transition Metal Carbonitride Ti3CNTx (MXene). *Science* **2020**, *369* (6502), 446.
(183) Duan, H.; Zhu, H.; Gao, J.; Yan, D.-X.; Dai, K.; Yang, Y.; Zhao, G.; Liu, Y.; Li, Z.-M. Asymmetric Conductive Polymer Composite Foam for Absorption Dominated Ultra-Efficient Electromagnetic Interference Shielding with Extremely Low Reflection Characteristics. *J. Mater. Chem. A* **2020**, *8* (18), 9146−9159.
(184) Zhou, B.; Su, M.; Yang, D.; Han, G.; Feng, Y.; Wang, B.; Ma, J.; Ma, J.; Liu, C.; Shen, C. Flexible MXene/Silver Nanowire-Based Transparent Conductive Film with Electromagnetic Interference Shielding and Electro-Photo-Thermal Performance. *ACS Appl. Mater. INTERFACES* **2020**, *12* (36), 40859−40869.
(185) Liang, C.; Ruan, K.; Zhang, Y.; Gu, J. Multifunctional Flexible Electromagnetic Interference Shielding Silver Nanowires/Cellulose Films with Excellent Thermal Management and Joule Heating Performances. *ACS Appl. Mater. INTERFACES* **2020**, *12* (15), 18023−18031.
(186) Song, P.; Qiu, H.; Wang, L.; Liu, X.; Zhang, Y.; Zhang, J.; Kong, J.; Gu, J. Honeycomb Structural rGO-MXene/Epoxy Nanocomposites for Superior Electromagnetic Interference Shielding Performance. *Sustain. Mater. Technol.* **2020**, *24*, e00153.
(187) Wei, Q.; Pei, S.; Qian, X.; Liu, H.; Liu, Z.; Zhang, W.; Zhou, T.; Zhang, Z.; Zhang, X.; Cheng, H.-M.; Ren, W. Superhigh Electromagnetic Interference Shielding of Ultrathin Aligned Pristine Graphene Nanosheets Film. *Adv. Mater.* **2020**, DOI: 10.1002/adma.201907411.
(188) Sheng, A.; Ren, W.; Yang, Y.; Yan, D.-X.; Duan, H.; Zhao, G.; Liu, Y.; Li, Z.-M. Multilayer WPU Conductive Composites with Controllable Electro-Magnetic Gradient for Absorption-Dominated Electromagnetic Interference Shielding. *Compos. PART -Appl. Sci. Manuf.* **2020**, *129*, 105692.
(189) Fan, Z.; Wang, D.; Yuan, Y.; Wang, Y.; Cheng, Z.; Liu, Y.; Xie, Z. A Lightweight and Conductive MXene/Graphene Hybrid Foam for Superior Electromagnetic Interference Shielding. *Chem. Eng. J.* **2020**, *381*, 122696.
(190) Hu, P.; Lyu, J.; Fu, C.; Gong, W.; Liao, J.; Lu, W.; Chen, Y.; Zhang, X. Multifunctional Aramid Nanofiber/Carbon Nanotube Hybrid Aerogel Films. *ACS Nano* **2020**, *14* (1), 688−697.
(191) Jin, X.; Wang, J.; Dai, L.; Liu, X.; Li, L.; Yang, Y.; Cao, Y.; Wang, W.; Wu, H.; Guo, S. Flame-Retardant Poly(Vinyl Alcohol)/MXene Multilayered Films with Outstanding Electromagnetic Interference Shielding and Thermal Conductive Performances. *Chem. Eng. J.* **2020**, *380*, 122475.
(192) Zhang, Y.; Ruan, K.; Shi, X.; Qiu, H.; Pan, Y.; Yan, Y.; Gu, J. Ti3C2Tx/rGO Porous Composite Films with Superior Electromagnetic Interference Shielding Performances. *CARBON* **2021**, *175*, 271−280.
(193) Li, Y.; Xue, B.; Yang, S.; Cheng, Z.; Xie, L.; Zheng, Q. Flexible Multilayered Films Consisting of Alternating Nanofibrillated Cellulose/Fe3O4 and Carbon Nanotube/Polyethylene Oxide Layers for Electromagnetic Interference Shielding. *Chem. Eng. J.* **2021**, *410*, 128356.
(194) Zhang, Y.; Xu, M.-K.; Wang, Z.; Zhao, T.; Liu, L.-X.; Zhang, H.-B.; Yu, Z.-Z. Strong and Conductive Reduced Graphene Oxide-MXene Porous Films for Efficient Electromagnetic Interference Shielding. *NANO Res.* **2022**, *15* (6), 4916−4924.
(195) Liu, K.; Liu, W.; Li, W.; Duan, Y.; Zhou, K.; Zhang, S.; Ni, S.; Xu, T.; Du, H.; Si, C. Strong and Highly Conductive Cellulose Nanofibril/Silver Nanowires Nanopaper for High Performance Electromagnetic Interference Shielding. *Adv. Compos. Hybrid Mater.* **2022**, *5* (2), 1078−1089.
(196) Song, P.; Ma, Z.; Qiu, H.; Ru, Y.; Gu, J. High-Efficiency Electromagnetic Interference Shielding of rGO@FeNi/Epoxy Composites with Regular Honeycomb Structures. *Nano-Micro Lett.* **2022**, DOI: 10.1007/s40820-022-00798-5.
(197) Wang, G.; Zhao, Y.; Yang, F.; Zhang, Y.; Zhou, M.; Ji, G. Multifunctional Integrated Transparent Film for Efficient Electromagnetic Protection. *Nano-Micro Lett.* **2022**, DOI: 10.1007/s40820-022-00810-y.
(198) Xie, Y.; Liu, S.; Huang, K.; Chen, B.; Shi, P.; Chen, Z.; Liu, B.; Liu, K.; Wu, Z.; Chen, K.; Qi, Y.; Liu, Z. Ultra-Broadband Strong Electromagnetic Interference Shielding with Ferromagnetic Graphene Quartz Fabric. *Adv. Mater.* **2022**, DOI: 10.1002/adma.202202982.
(199) Ma, L.; Hamidinejad, M.; Zhao, B.; Liang, C.; Park, C. B. Layered Foam/Film Polymer Nanocomposites with Highly Efficient EMI Shielding Properties and Ultralow Reflection. *Nano-Micro Lett.* **2022**, DOI: 10.1007/s40820-021-00759-4.
(200) Shi, Y.; Xiang, Z.; Cai, L.; Pan, F.; Dong, Y.; Zhu, X.; Cheng, J.; Jiang, H.; Lu, W. Multi-Interface Assembled N-Doped MXene/HCFG/AgNW Films for Wearable Electromagnetic Shielding Devices with Multimodal Energy Conversion and Healthcare Monitoring Performances. *ACS Nano* **2022**, *16* (5), 7816−7833.
(201) Fan, B.; Xing, L.; Yang, K.; Yang, Y.; Zhou, F.; Tong, G.; Wu, W. Salt-Templated Graphene Nanosheet Foams Filled in Silicon Rubber toward Prominent EMI Shielding Effectiveness and High Thermal Conductivity. *CARBON* **2023**, *207*, 317−327.
(202) Anand, S.; Vu, M. C.; Mani, D.; Kim, J.-B.; Jeong, T.-H.; Islam, Md. A.; Kim, S.-R. Dual 3D Networks of Graphene Derivatives Based Polydimethylsiloxane Composites for Electrical Insulating Electronic Packaging Materials with Outstanding Electromagnetic Interference Shielding and Thermal Dissipation Performances. *Chem. Eng. J.* **2023**, *462*, 142017.

(203) Shu, J.-C.; Wang, Y.-Z.; Cao, M.-S. PEDOT:PSS-Patched Magnetic Graphene Films with Tunable Dielectric Genes for Electromagnetic Interference Shielding and Infrared Stealth. *J. Mater. Sci. Technol.* **2024**, *186*, 28−36.
(204) Wyatt, B. C.; Nemani, S. K.; Anasori, B. 2D Transition Metal Carbides (MXenes) in Metal and Ceramic Matrix Composites. *Nano Converg.* **2021**, *8* (1), 16.
(205) Frey, N. C.; Wang, J.; Vega Bellido, G. I.; Anasori, B.; Gogotsi, Y.; Shenoy, V. B. Prediction of Synthesis of 2D Metal Carbides and Nitrides (MXenes) and Their Precursors with Positive and Unlabeled Machine Learning. *ACS Nano* **2019**, *13* (3), 3031−3041.
(206) Wang, Y.; Nian, Y.; Biswas, A. N.; Li, W.; Han, Y.; Chen, J. G. Challenges and Opportunities in Utilizing MXenes of Carbides and Nitrides as Electrocatalysts. *Adv. Energy Mater.* **2021**, *11* (3), 2002967.
(207) Bao, Y.; Guo, S.; Li, Y.; Jia, Z.; Guan, H.; Lei, D.; Chen, J.; Zhong, B.; Li, Z. Lightweight Honeycomb rGO/$Ti_3C_2T_x$ MXene Aerogel without Magnetic Metals toward Efficient Electromagnetic Wave Absorption Performance. *ACS Appl. Electron. Mater.* **2023**, *5* (1), 227−239.
(208) Liang, L.; Li, Q.; Yan, X.; Feng, Y.; Wang, Y.; Zhang, H.-B.; Zhou, X.; Liu, C.; Shen, C.; Xie, X. Multifunctional Magnetic $Ti_3C_2T_x$ MXene/Graphene Aerogel with Superior Electromagnetic Wave Absorption Performance. *ACS Nano* **2021**, *15* (4), 6622−6632.
(209) Cai, Y.; Xu, L.; Pan, H.; Yao, C.; Li, Y.; Hu, L.; Zhao, H.; Yang, Q.; Wang, L.; Shen, Y. Preparation of Three-Dimensional Multilayer Flower-like Structured MoS2/RGO Composites with Enhanced Microwave Absorption. *J. Mater. Sci.* **2025**, *60* (6), 2832−2847.
(210) Yang, Z.; Wang, B.; Wei, S.; Wang, X.; Wang, Y.; Liang, Y.; Liu, Z. Fe/MoS2/Graphite Lamellar Composites: Ultra-Thin Electromagnetic Wave Absorbers with Mass Production Potential. *J. Alloys Compd.* **2025**, *1025*, 180367.
(211) Guo, Z.; Ren, P.; Yang, F.; Wu, T.; Zhang, L.; Chen, Z.; Huang, S.; Ren, F. MOF-Derived Co/C and MXene *Co* -Decorated Cellulose-Derived Hybrid Carbon Aerogel with a Multi-Interface Architecture toward Absorption-Dominated Ultra-Efficient Electromagnetic Interference Shielding. *ACS Appl. Mater. Interfaces* **2023**, *15* (5), 7308−7318.

https://doi.org/10.1021/acsaenm.5c00207
ACS Appl. Eng. Mater. 2025, 3, 2234−2258